Implicit-Explicit Runge-Kutta schemes for hyperbolic systems and kinetic equations in the diffusion limit

S. Boscarino[*] L. Pareschi[†] G.Russo[‡]

October 21, 2011

Abstract

We consider Implicit-Explicit (IMEX) Runge-Kutta schemes for hyperbolic and kinetic equations in the diffusion limit. In such regime the system relaxes towards a parabolic convection-diffusion equation and it is desirable to have a method that is able to capture the asymptotic behavior with an implicit treatment of the limiting diffusive terms. To this goal we reformulate the problem by properly combining the limiting diffusion flux with the convective flux. This, however, introduces new difficulties due to the dependence of the stiff source term on the gradient. Thus, by an accurate analysis of the different type of IMEX schemes, we proposed several schemes that under some assumptions show good behavior with respect to the small scaling parameter in the zero relaxation limit. In particular, at variance with the classical fluid-limit, our approach originates in the zero relaxation limit an IMEX method for the corresponding convection-diffusion system. Several numerical examples including neutron transport equations confirm the theoretical analysis.

Key words. IMEX Runge-Kutta methods, hyperbolic conservation laws with sources, transport equations, diffusion equations, stiff systems.

AMS subject classification. 65C20, 65M06, 76D05, 82C40.

Contents

[*]Mathematics and Computer Science Department, University of Catania, Italy (boscarino@dmi.unict.it).
[†]Mathematics Department, University of Ferrara, Italy (lorenzo.pareschi@unife.it).
[‡]Mathematics and Computer Science Department, University of Catania, Italy (russo@dmi.unict.it).

1 Introduction

The development of numerical methods to solve hyperbolic systems in diffusive regimes has been a very active area of research in the last years (see for example [20, 23, 26, 29]).

Classical fields of applications involve diffusion in neutron transport [7, 14, 15, 21, 27], drift-diffusion limit in semiconductors [22, 25] and incompressible Navier-Stokes limits in rarefied gas dynamic [24]. A strictly related field of research concerns the construction of schemes for the compressible Navier-Stokes limit (see [2] and the references therein). In such physical problems, the scaling parameter (mean free path) may differ in several orders of magnitude from the rarefied regimes to the diffusive regimes, and it is desirable to develop a class of robust numerical schemes that can work uniformly with respect to this parameter.

A prototype hyperbolic system of conservation laws with diffusive relaxation that we will use to illustrate the subsequent theory is the following, [20, 22, 29]

$$\begin{aligned} &u_t + v_x = 0, \\ &v_t + \frac{1}{\varepsilon^2} p(u)_x = -\frac{1}{\varepsilon^2}\left(v - q(u)\right), \end{aligned} \tag{1}$$

where $p'(u) > 0$. System (1) is hyperbolic with two distinct real characteristics speeds $\pm\sqrt{p'(u)}/\varepsilon$.

In the small relaxation limit, $\varepsilon \to 0$, the behavior of the solution to (1) is, at least formally, governed by the *convection-diffusion* equation

$$\begin{aligned} &u_t + q(u)_x = p(u)_{xx}, \\ &v = q(u) - p(u)_x. \end{aligned} \tag{2}$$

The so called subcharacteristic condition [13] for system (1) becomes

$$|q'(u)|^2 < \frac{p'(u)}{\varepsilon^2}, \tag{3}$$

and it is naturally satisfied in the limit $\varepsilon \to 0$.

In general, numerical approaches that work for hyperbolic system with stiff relaxation terms do not apply directly in the diffusive scaling since in these systems we have the presence of multiple time-scales. In fact, together with the stiff relaxation term we have a stiff convection therm that contributes to the asymptotic diffusive behavior. Then special care must be taken to ensure that the schemes possess the correct zero-relaxation limit, in the sense that the numerical scheme applied to system (1) should be a consistent and stable scheme for the limit system (2) as the parameter ε approaches zero. A notion usually referred to as *asymptotic preservation*.

IMEX Runge-Kutta (R-K) schemes [1, 3, 4, 9, 31] represent a powerful tool for the time discretization of such stiff systems. Unfortunately, since the characteristic speed of the hyperbolic part is of order $1/\varepsilon$, standard IMEX R-K schemes developed for hyperbolic systems with stiff relaxation [31, 6] become useless in such parabolic scaling, because the CFL condition would require $\Delta t = \mathcal{O}(\varepsilon \Delta x)$. Of course, in the diffusive regime where $\varepsilon < \Delta x$, this is very restrictive since for an explicit method a parabolic condition $\Delta t = \mathcal{O}(\Delta x^2)$ should suffice.

Most previous works on asymptotic preserving schemes for hyperbolic systems and kinetic equations with diffusive relaxation focus on schemes which in the limit of infinite stiffness become consistent explicit schemes for the diffusive limit equation [20, 23, 26, 27, 29]. Such explicit schemes clearly suffer from the usual stability restriction $\Delta t = \mathcal{O}(\Delta x^2)$. Schemes that avoid such time step restriction and provide fully implicit solvers in the case of transport equations have been analyzed in [7].

In this paper we present a general methodology to tackle such difficulties which applies to a broad class of problems. The idea is to reformulate problem (1) by properly combining the limiting diffusion flux with the convective flux. This allow to construct a class of IMEX R-K schemes that work with high order accuracy in time and that, in the diffusion limit (i.e. when $\varepsilon \to 0$), originate an IMEX method for the limiting convection-diffusion equation (2). Related reformulations with the goal to obtain asymptotic-preserving methods have been proposed in [20, 19].

Our new approach guarantees to use a CFL hyperbolic condition $\Delta t = \mathcal{O}(\Delta x)$ independent of ε when applied to (1) in all regimes. The aim of this paper is to derive and analyze different types of IMEX R-K schemes when applied to the reformulated problem in the stiff regime ($\varepsilon \to 0$).

The rest of the paper is organized as follows. The next section provides the bases of the numerical method and the analysis of the different IMEX R-K schemes. In particular, following [6], we prove that under suitable assumptions the new IMEX R-K methods are consistent with the diffusion limit. In Section 3 we describe space discretization obtained by conservative finite difference schemes. Numerical results of the proposed IMEX R-K schemes are presented in section 4. In Section 5 we apply the method to the one-dimensional Newton transport equation and present several numerical results and comparison with previous methods. Additional technical material, like the index 1 order conditions, is given in the separate Appendices.

2 IMEX Runge-Kutta schemes for diffusive relaxation problems

The starting point is to reformulate problem (1) as the equivalent system

$$\begin{aligned} u_t &= -(v + \mu p(u)_x)_x + \mu p(u)_{xx}, \\ \varepsilon^2 v_t &= -p(u)_x - v + q(u), \end{aligned} \tag{4}$$

where the therm $\mu p(u)_{xx}$ has been added and subtracted to the first equation in (1). Here $\mu = \mu(\varepsilon) \in [0, 1]$ is a free parameter such that $\mu(0) = 1$. The idea is that, since the quantity $v+p(u)_x$ is close to $q(u)$ as $\varepsilon \to 0$, the first term on the right hand side can be treated explicitly in the first equation, while the therm $p(u)_{xx}$ will be treated implicitly. This can be done naturally by using an Implicit-Explicit approach, as we will explain later. Let us point out that the choice $\mu \equiv 1$, as shown in Appendix 1, guarantees the largest stability region of the method.

Next we will study the behavior of the different IMEX R-K schemes when applied to the evolution system (4) in the diffusion limit. In particular we will show that no parabolic stability restriction on the time step appears in the diffusive limit.

2.1 Diffusion limit and Differential Algebraic Equations (DAE)

System (4) can be written in the form

$$\begin{aligned} u' &= f_1(u,v) + f_2(u), \\ \varepsilon^2 v' &= g(u,v) \end{aligned} \tag{5}$$

where the primes denote the time derivatives and

$$f_1(u,v) = -\partial_x(v + \mu\partial_x p(u)), \quad f_2(u) = \mu\partial_{xx}p(u),$$

$$g_1(u,v) = -\partial_x p(u) - v + q(u).$$

Then it is natural to consider a direct application of an IMEX-RK scheme to the previous system where $(f_1(u,v),0)^T$ is evaluated explicitly and $(f_2(u),g(u,v))^T$ implicitly. Note that if $f_2(u)$ is evaluated explicitly then by cancellation the IMEX-RK scheme will reduce to the typology of asymptotic preserving methods studied in [5, 30].

Setting $f(u,v) = f_1(u,v) + f_2(u)$ system (5) takes the form of a classical of a singularly perturbation problem [17]

$$\begin{aligned} u' &= f(u,v), \\ \varepsilon^2 v' &= g(u,v). \end{aligned} \tag{6}$$

In the limit $\varepsilon \to 0$ we obtain a differential algebraic system (DAE)

$$\begin{aligned} u' &= f(u,v), \\ 0 &= g(u,v). \end{aligned} \tag{7}$$

In order to guarantee the solvability of system (7) we assume that the Jacobian matrix $g_v(u,v)$ is invertible, and then the DAE is said to be of index 1 [1]. Note that if g_v has a bounded inverse in a neighborhood of the exact solution, we can use the inverse function theorem in order to writhe

$$v(t) = G(t, u(t))$$

for some $G(t,u)$ which inserted into $u' = f(u,v)$ gives $u' = f(u,G(u))$. From now on we always assume that this is the case.

Then, as $\varepsilon \to 0$ system (5) reduces to

$$u' = \hat{f}_1(u) + f_2(u), \tag{8}$$

where $\hat{f}_1(u) = f_1(u,G(u))$ and $v = G(u)$.

Boscarino in [3] has developed an accurate analysis of problem (6), showing that different types of IMEX R-K schemes suffer from the phenomenon of order reduction in the stiff regime $(\Delta t \gg \varepsilon)$ when the classical order is greater than two, and the observed convergence rates of the methods drop the order of accuracy in time. Subsequently in [4, 6] a new class of IMEX RK schemes for solving hyperbolic systems with relaxation has been developed by imposing extra order conditions in addition to the classical ones [9, 31]. Then it is natural to apply the same kind of analysis to the construction of IMEX schemes for the diffusive relaxation systems.

[1] The index of a DAE is the number of times one has to differentiate the function g to obtain a system of ODE's. For example, differentiating the function g, one obtains $g_u(u,v)u' + g_v(u,v)v' = 0$. If g_v is invertible, system (7) can be written as $u' = f(u,v)$, $v' = -g_v' g_u f$.

2.2 Classification and analysis of IMEX R-K methods

IMEX Runge-Kutta schemes have been widely used in the literature to treat problems that contain both stiff and non stiff terms [1, 9, 31]. The stiff terms are treated implicitly, while the non stiff terms are treated explicitly, thus lowering the computational complexity of the scheme.

Applying an IMEX Runge-Kutta scheme to system (5) we obtain

$$\begin{aligned} u_{n+1} &= u_n + \Delta t \sum_{k=1}^{s} \tilde{b}_k f_1(U_k, V_k) + \Delta t \sum_{k=1}^{s} b_k f_2(U_k) \\ \varepsilon^2 v_{n+1} &= \varepsilon^2 v_n + \Delta t \sum_{k=1}^{s} b_k g(U_k, V_k), \end{aligned} \tag{9}$$

for the numerical solution and

$$\begin{aligned} U_k &= u_n + \Delta t \sum_{j=1}^{k-1} \tilde{a}_{kj} f_1(U_k, V_k) + \Delta t \sum_{j=1}^{k} a_{kj} f_2(U_k) \\ \varepsilon^2 V_k &= \varepsilon^2 v_n + \Delta t \sum_{j=1}^{k} a_{kj} g(U_j, V_j), \end{aligned} \tag{10}$$

for the internal stages.

Here the $s \times s$ matrices $\tilde{A} = (\tilde{a}_{ij})$, $A = (a_{ij})$ and the vectors $\tilde{b}$, $b \in \mathbb{R}^s$ characterize the scheme, and can be represented by a double *tableau* in the usual Butcher notation

$$\begin{array}{c|c} \tilde{c} & \tilde{A} \\ \hline & \tilde{b}^T \end{array} \qquad \begin{array}{c|c} c & A, \\ \hline & b^T \end{array}.$$

The coefficients $\tilde{c}$ and c are used if the right hand side depends explicitly on time. We assume that they satisfy the usual relation

$$\tilde{c}_i = \sum_{j=1}^{i-1} \tilde{a}_{ij}, \quad c_i = \sum_{j=1}^{i} a_{ij}. \tag{11}$$

Matrix $\tilde{A}$ is lower triangular with zero diagonal, while matrix A is lower triangular, i.e. the implicit scheme is a diagonally implicit Runge-Kutta (DIRK), this choice guarantees that function f_1 is always explicitly evaluated.

IMEX R-K schemes presented in the literature can be classified in two main different types characterized by the structure of the matrix $A = (a_{ij})_{i,j=1}^{s}$ of the implicit scheme.

Definition 1 *We call an IMEX R-K method of type A (see [31]) if the matrix $A \in \mathbb{R}^{s \times s}$ is invertible.*

Definition 2 *We call an IMEX R-K method of type CK (see [9]) if the matrix $A \in R^{s \times s}$ can be written as*

$$A = \begin{pmatrix} 0 & 0 \\ a & \hat{A} \end{pmatrix}$$

with $a \in \mathbb{R}^{(s-1)}$ and the submatrix $\hat{A} \in \mathbb{R}^{(s-1) \times (s-1)}$ invertible. In the special case $a = 0$ the scheme is said to be of type ARS (see [1]).

In the sequel we restrict our analysis to the limit case $\varepsilon \to 0$ where the main goal is to capture the diffusive limit.

Analysis of TYPE A schemes. Starting from (9) and (10), by Definition (1) we suppose A invertible and obtain from the second equation in (10)

$$\Delta t g(U_i, V_i) = \varepsilon^2 \sum_{j=1}^{k} \omega_{ij}(V_j - v_n),$$

where ω_{kj} are the elements of the inverse of A^{-1}. Inserting this into the numerical solution v_{n+1} we make the definition of v_{n+1} independent of ε^2 and putting $\varepsilon = 0$, we get

$$\begin{aligned} u_{n+1} &= u_n + \Delta t \sum_{k=1}^{s} \tilde{b}_k \hat{f}_1(U_k) + \Delta t \sum_{k=1}^{s} b_k f_2(U_k) \\ v_{n+1} &= R(\infty) v_n + \Delta t \sum_{k=1}^{s} b_k \omega_{kj} V_j, \end{aligned} \tag{12}$$

with $\hat{f}_1(U_k) = f_1(U_k, G(U_k))$, and stage values

$$\begin{aligned} U_k &= u_n - \Delta t \sum_{j=1}^{k-1} \tilde{a}_{kj} \hat{f}_1(U_j) - \Delta t \sum_{j=1}^{k} a_{kj} f_2(U_j) \\ 0 &= g(U_k, V_k). \end{aligned} \tag{13}$$

for $k = 1, \ldots, s$. The latter equality implies $V_k = G(U_k)$, $k = 1, \ldots, s$.

In (12) we denoted by

$$R(\infty) = 1 - b^T A^{-1} \mathbf{1} = \lim_{z \to \infty} R(z),$$

where $R(z)$ is *the stability function* of the implicit scheme defined by (see [17], Sect. IV.3)

$$R(z) = 1 + z b^T (I - zA)^{-1} \mathbf{1},$$

with $b^T = (b_1, \ldots, b_s)$ and $\mathbf{1} = (1, \ldots, 1)^T$.
Note that if we require that the implicit part of the scheme is *stiffly accurate*, i.e.

$$b^T A^{-1} = e_s^T,$$

where $e_s = (0, \ldots, 0, 1)^T$, then

$$R(\infty) = 1 - b^T A^{-1} \mathbf{1} = 1 - e_s^T \mathbf{1} = 1 - 1 = 0.$$

This implies that if the implicit scheme is A-stable, it is also L-stable and

$$v_{n+1} = V_s = G(U_s).$$

Clearly the numerical solution (u_{n+1}, v_{n+1}) of the above approach in the case $\varepsilon = 0$ will not lie on the manifold $g(u, v) = 0$ since $g(u_{n+1}, v_{n+1}) \neq 0$. However, it is interesting to note that, if we consider system (4) in the case $q(u) = 0$ then in the limit $\varepsilon = 0$ we get a purely diffusive system which means that the term $f_2(u)$ in (5) disappears. Therefore the scheme becomes a stiffly accurate DIRK scheme and hence $u_{n+1} = U_s$, implying $g(u_{n+1}, v_{n+1}) = 0$.

Of course, in the general case of systems for which $f_2(u) \neq 0$ in the limit case $\varepsilon \to 0$ it is not true that $g(u_{n+1}, v_{n+1}) = 0$ even if all stage values lie on the manifold. However, if the explicit scheme has the property that $u_{n+1} = U_s$, and the implicit scheme is stiffly accurate, then, in the limit as $\varepsilon \to 0$ the numerical solutions are projected on the manifold $g(u_{n+1}, v_{n+1}) = 0$.

From the above discussion it is clear that the property $u_{n+1} = U_s$ is essential if we want that the numerical solution is projected to the limit manifold as $\varepsilon \to 0$. This motivate the following definition, which is a generalization of the stiffly accurate property.

Definition 3 *We say that a IMEX R-K scheme is* stiffly accurate *if* $b^T = e_s^T A$ *and* $\tilde{b}^T = e_s^T \tilde{A}$, *with* $e_s = (0, \ldots, 0, 1)^T$, *and* $c_s = \tilde{c}_s = 1$, *i.e. the numerical solution is identical to the last internal stage value of the scheme.*

From (9) and (10) we observe that if an IMEX R-K is stiffly accurate in the sense of Definition (3), then $u_{n+1} = U_s$, $v_{n+1} = V_s$, and therefore $\lim_{\varepsilon \to 0} g(u_{n+1}, v_{n+1}) = 0$. However some remarks are in order.

Remark 1

- *We introduced definition 3 as an extension to IMEX Runge-Kutta schemes of the standard definition of stiff accuracy given for implicit Runge-Kutta methods. In the literature the special class of s-stage explicit Runge-Kutta schemes for which the coefficients have a special structure, i.e.,* $a_{s,i} = b_i$ *for* $i = 1, \ldots, s-1$ *and* $b_s = 0$, *is called* First Same As Last *(FSAL). Such schemes have the advantage that they require* $s-1$ *function evaluation for each step, (see [18] for details). Then using this definition, we may say that a IMEX R-K scheme is* stiffly accurate *if the implicit scheme is stiffly accurate and the explicit scheme is FSAL.*

- *It is worth mentioning two important aspects about type A schemes. First of all, in [3] Boscarino emphasized that an important ingredient for the IMEX R-K schemes of type A is* $b_i = \tilde{b}_i$ *for all* i. *Such a choice provides a significant benefit for the differential u-component, i.e., an order reduction does not appear for this component. On the other hand, conditions*
$$e_s^T \tilde{A} = \tilde{b}^T, \quad e_s^T A = b^T$$
imply $a_{ss} = b_s \neq \tilde{b}_s = \tilde{a}_{ss} = 0$ *which means that for a stiffly accurate IMEX R-K scheme it is* $b \neq \tilde{b}$, *and therefore we expect to observe order reduction for the differential variable.*

- *It is impossible to construct a second order stiffly accurate IMEX Runge-Kutta scheme of type A with* $s = 3$ *internal stages. The proof is given in Appendix 2. In practice, in order to satisfy all these order conditions we have to increase the number of the internal stages. In view of such difficulties, from now on, we shall consider second order IMEX R-K schemes of type A with* $s = 3$ *and* $\tilde{b}_i = b_i$ *for all* i *in order to avoid the order reduction, giving up to the FSAL property of the explicit scheme (and with that the stiffly accurate of the IMEX scheme).*

- *Finally we observe that, in order to construct an order* $p \geq 3$ *IMEX R-K of type A and to maintain accuracy we have to increase the number of the classical order conditions too. Usually several simplifying assumptions (see [4], [6], [17] for details) could help us to reduce the number of such conditions, but, for larger orders type A schemes are more complicated to construct than CK or ARS schemes because of additional order conditions (see [6]).*

Analysis of TYPE CK schemes. IMEX CK schemes [9] are attractive because in general they do not require $b = \tilde{b}$ in order to avoid order reduction in the differential variable in the limit $\varepsilon \to 0$, [3]. Because of this, it is easier to construct stiffly accurate schemes according to definition 3, such schemes will project the solution on the manifold in the limit of infinite stiffness.

Now we analyze IMEX R-K schemes of type CK where, by Definition 2, we assume that the submatrix $\hat{A}$ is invertible and $a_{11}=0$. The Butcher tableaux of a CK scheme takes the form

$$\begin{array}{c|cc} 0 & 0 & 0 \\ \hat{c} & a & \hat{A} \\ \hline & b_1 & \hat{b}^T \end{array}$$

with $a=(a_{21},\dots,a_{s,1})^T$ and $\hat{b}^T=(b_2,\dots,b_s)$. In order to simplify the analysis we consider that the implicit part of the scheme is stiffly accurate. Under this circumstance it is easy to prove that $b_1+\hat{b}^T\alpha=0$, where $\alpha\equiv-\hat{A}^{-1}a$ (see [3] for details).

Then, considering a scheme of the type CK, the second equation in (10) becomes

$$\varepsilon^2 V_l=\varepsilon^2 v_n+\Delta t a_{l1} g(u_n,v_n)+\Delta t\sum_{j=2}^{l} a_{lj} g(U_j,V_j).$$

Now multiplying by $\hat{\omega}_{kl}$, where $\hat{\omega}_{kj}$ are the elements of the inverse of $\hat{A}$, and summing on l, we obtain

$$\Delta t g(U_k,V_k)=\varepsilon^2\sum_{j=2}^{s}\hat{\omega}_{kj}(V_j-v_n)+\Delta t\alpha_k g(u_n,v_n),\quad \text{for}\quad k=2,\dots,s$$

where

$$\sum_{l=2}^{s}\hat{\omega}_{kl}a_{lj}=\delta_{kj},\qquad -\sum_{l=2}^{s}\hat{\omega}_{kl}a_{l1}=\alpha_k.$$

Inserting the expression for $\Delta t g(U_k,V_k)$ into the second equation in (9) we obtain for the numerical solutions

$$\begin{aligned} u_{n+1} &= u_n+\Delta t\left(\tilde{b}_1 f_1(u_n,v_n)+\sum_{k=2}^{s}\tilde{b}_k f_1(U_k,V_k)+b_1 f_2(u_n)+\sum_{k=2}^{s} b_k f_2(U_k)\right) \\ \varepsilon^2 v_{n+1} &= \varepsilon^2 R(\infty)v_n+\varepsilon^2\Delta t\sum_{k=2}^{s} b_k\omega_{kj}V_j+\Delta t\left(b_1+\sum_{k=2}^{s} b_k\alpha_k\right)g(u_n,v_n) \end{aligned}\tag{14}$$

with

$$U_k = u_n+\Delta t\left(\tilde{a}_{k1} f_1(u_n,v_n)+\sum_{j=2}^{k-1}\tilde{a}_{kj} f_1(U_j,V_j)+a_{k1} f_2(u_n)+\sum_{j=1}^{k} a_{kj} f_2(U_j)\right).\tag{15}$$

Then the last term in the second equation in (14) drops and in the limit case for $\varepsilon=0$ we can write

$$v_{n+1} = R(\infty)v_n+\Delta t\sum_{k=2}^{s} b_k\omega_{kj}V_j,$$

with

$$g(U_k,V_k) = \alpha_k g(u_n,v_n),\quad \text{for}\quad k=2,\dots,s.$$

Note that, for IMEX R-K schemes of type CK, the stability function $R(z)$ of the implicit part of the scheme takes the form

$$
\begin{aligned}
R(z) &= 1 + z(b_1 + \hat{b}^T (I - z\hat{A})^{-1}(\mathbf{1}_{s-1} + za)) \\
&= (b_1 - \hat{b}^T \hat{A}^{-1} a) z + (1 - \hat{b}^T \hat{A}^{-1}\mathbf{1}_{s-1} + \hat{b}^T \hat{A}^{-2} a) + \mathcal{O}(\frac{1}{z}).
\end{aligned} \tag{16}
$$

We obtained this result, by applying one step of the implicit part of the scheme to the test problem $y' = \lambda y$, $y(t_0) = 1$, with $\lambda \in \mathbb{C}$ and $\mathbf{1}_s = (1, \dots, 1)^T \in \mathbb{R}^s$.

Thus, the only stiffly accurate condition, i.e. $\hat{e}_{s-1}^T \hat{A} = \hat{b}^T$ is not enough to guarantee that $lim_{z\to\infty} R(z) = 0$ and then an additional condition is required for the implicit part of the scheme, (for details see [6]). This is expressed by the following

Proposition 1 *If*

$$
-\hat{e}_{s-1}^T \hat{A}^{-1} a = \sum_{j\geq 2} \hat{\omega}_{sj} a_{j1} = 0, \tag{17}
$$

then $R(\infty) = 0$, *where* $\hat{e}_{s-1} = (0, \dots, 0, 1)^T \in \mathbb{R}^{s-1}$.

Proof. In fact, assuming $\hat{A}$ invertible, we get $\hat{b}^T \hat{A}^{-1} = \hat{e}_{s-1}^T$ and when $z \to \infty$, from (16) we obtain $R(\infty) = \hat{b}^T \hat{A}^{-2} a = -\hat{e}_{s-1}^T \hat{A}^{-1} a$, which is zeros if (17) is satisfied. □
Note that the previous Lemma implies that $\alpha_s = -\hat{e}_{s-1}^T \hat{A}^{-1} a = 0$ then the last stage values lie on the manifold $g(u, v) = 0$ as $\varepsilon \to 0$.
From (14) and (15) we observe that if the IMEX R-K scheme of type CK is stiffly accurate in the sense of Definition (3), then we obtain again $u_{n+1} = U_s$ and $v_{n+1} = V_s$ and therefore $g(u_{n+1}, v_{n+1}) = 0$ with $v_{n+1} = G(u_{n+1})$.

Since an IMEX R-K schemes of type ARS is a particular case of the type CK where the vector $a = 0$, then the same results hold true.

2.3 Algebraic order condition for index 1 DAEs

Formulation (5) in the limit case $\varepsilon \to 0$ yields the index-1 DAEs. Then using the same technique adopted in [4], we can derive additional order conditions, called *algebraic conditions*, that guarantee the correct behavior of the numerical solution in the limit $\varepsilon \to 0$ and maintain the accuracy in time of the scheme.

Here we introduce algebraic order conditions for the type A IMEX R-K schemes (12)-(13). For completeness, in Appendix 3 we report such conditions, applied to the system (8). Then, the additional algebraic order conditions for index 1 DAEs up to third order are the following

$$
b^T A^{-1} \tilde{c} = 1, \quad b^T A^{-1} \tilde{c}^2 = 1, \quad b^T A^{-1} \tilde{A} \tilde{c} = 1/2, \tag{18}
$$

where $\tilde{c} = \tilde{A} e$ with $e = (1, \dots, 1)^T$. For the type CK (consequently for the type ARS) we can rewrite these algebraic order conditions replacing A^{-1} with $\hat{A}^{-1}$. We observe that in the limit case $\varepsilon \to 0$, the original system relaxes to the DAEs (7), and the numerical scheme becomes an IMEX scheme for the limit equation (8) for the variable u. This is different from what is usually obtained when applying IMEX schemes to hyperbolic relaxation problems. In that case, the IMEX scheme relaxes to an explicit scheme for the underlying equation for the variable u (see [31]).

3 IMEX-Finite Difference schemes

When constructing numerical schemes, one has also to take a great care in order to avoid spurious numerical oscillations arising near discontinuities of the solution. This is avoided by a suitable choice of space discretization. To this aim it is necessary to use non-oscillatory interpolating algorithms, in order to prevent the onset of spurious oscillations (like ENO and WENO methods), see [34]. Moreover the choice of the space discretization my be relevant for a correct treatment of the boundary conditions.

In this section we emphasize some requirements about the space discretization of the system (4). We remark that the dissipative nature of upwind schemes [29, 30] depends essentially on the fact that the characteristic speeds of the hyperbolic part are proportional to $1/\varepsilon$. On the other hand central differences schemes avoid excessive dissipation but when ε is not small or when the limiting equations contain advection terms may lead to unstable discretizations. In order to overcome these well-known facts and to have the correct asymptotic behaviour we fix some general requirements for the space discretization.

1. *Correct diffusion limit.* Let us consider system (4) with $q(u) = 0$. In the limit case $\varepsilon \to 0$ the therm $v + \partial_x p(u) \to 0$ from the second equation. If we want that $v + \mu(\varepsilon)\partial_x p(u) \to 0$ also in the first equation, we need to use the same space discretization for the term $\partial_x p(u)$ and require that $\mu(0) = 1$.

2. *Compact stencil.* Among the advantages of our approach there is the possibility to have a scheme with a compact stencil in the diffusion limit $\varepsilon \to 0$. This property is satisfied if point 1) is satisfied and we use a suitable discretization for the second order derivative that characterize the diffusion limit.

3. *Shock capturing.* The schemes when $q(u) \neq 0$ should be based on shock capturing high order fluxes for the convection part. This is necessary not only for large values of ε but also when we consider convection-diffusion type limit equations with small diffusion. The high order fluxes are then necessary for all space derivatives except for the second order term $\mu(\varepsilon)\partial_{xx} p(u)$ on the right hands side.

4. *Avoid solving nonlinear algebraic equations.* In order to achieve this the implicit space derivative $\partial_x p(u)$ in the second equation must be evaluated using only nodal values of u which can be obtained from the solution of the first equation.

The above properties are satisfied for example using high accuracy in space obtained by finite difference discretization with Weighted-Essentially Non Oscillatory (WENO) reconstruction, [34].

The system may be written in the form

$$\begin{aligned} u_t + (v + \mu p(u)_x)_x &= \mu p(u)_{xx}, \\ v_t &= \frac{1}{\varepsilon^2}\left(q(u) - (v + p(u)_x)\right). \end{aligned} \tag{19}$$

The terms on the right hand side will be treated implicitly. For large value of ε the explicit flux is just $(v, 0)^T$, while for small values of ε it is $(v + p(u)_x, 0)^T$. Here we describe a finite difference WENO scheme for a system of the form

$$U_t + F(U)_x = G(U),$$

and apply it to the system (19) with

$$F(U) = (v + \mu p(u)_x, 0)^T,$$
$$G(U) = \left(\mu p(u)_{xx}, \frac{1}{\varepsilon^2}\left(q(u) - (v + p(u)_x)\right)\right).$$

As $\varepsilon \to \infty$ and $\mu \to 0$, the system becomes

$$\begin{aligned} u_t + v_x &= 0, \\ v_t &= 0 \end{aligned}$$

and the characteristic speeds of the system are $\lambda = 0, 1$. As $\varepsilon \to 0$ and $\mu \to 1$, $v + \mu p(u)_x \to q(u)$ and the system relaxes to the equation

$$u_t + q(u)_x = \mu p(u)_{xx}$$

and the characteristic speed of the left hand side is given by $\lambda = q'(u)$.

Conservative finite difference for system (19) are written as follows, [31]

$$\frac{dU_j}{dt} = -\frac{\hat{F}_{j+\frac{1}{2}} - \hat{F}_{j-\frac{1}{2}}}{\Delta x} + G(U_j)$$

where $U_j(t) \approx U(x_j, t)$ is an approximation of the pointwise value of U at grid nodes, and the numerical flux at cell edge $x_{j+\frac{1}{2}}$ is computed as follows

$$\hat{F}_{j+\frac{1}{2}} = \hat{F}^+_j(x_{j+\frac{1}{2}}) + \hat{F}^-_{j+1}(x_{j+\frac{1}{2}}).$$

The function $\hat{F}^+_j(x)$ and $\hat{F}^-_{j+1}(x)$ are suitable reconstructions defined, respectively, in cell j and in cell $j+1$. They are obtained as follows. First, we assume that the flux can be split into a positive and negative component

$$F(U) = F^+(U) + F^-(U),$$

with $\lambda(\Delta_U F^+(U)) \geq 0$, $\lambda(\Delta_U F^-(U)) \leq 0$. The quantity $F^\pm_j = F^\pm(U_j)$ are computed at cell center. Then $\hat{F}^\pm_j(x)$ are reconstructed from $\left\{F^\pm_j\right\}$ using high order essentially non oscillatory reconstruction, such as ENO or WENO, that allows pointwise reconstruction of a function from its cell averages, (see, e.g. [34] for details).

In all our examples we used the simple local Lax-Friedrix flux decomposition, i.e. $F^+(U) = \frac{1}{2}(F(U) + \alpha U)$, $F^-(U) = \frac{1}{2}(F(U) - \alpha U)$, $\alpha \geq \max_U |\rho(\Delta_U F)|$, $\forall A \in \mathbb{R}^{m\times m}$, where $\rho(A) = \max_{1\leq i\leq m} |\lambda_i(A)|$ denotes the spectral radius of matrix A, and the max defining α is taken for U varying in a suitable range in a neighborhood of each cell. In our test case we chose $\alpha = 1$, since as $\varepsilon \to \infty$, $\rho(\Delta_U F) = 1$ and in our numerical test $q(u)$ is either 0, u, or $u^2/2$, with U ranging in $[0, 1]$, therefore $|q'(u)| \leq 1$.

Furthermore for large value of ε, (e.g., $\varepsilon = 1$), we want to avoid adding and subtracting terms which may cause loss of accuracy. For such reason a simple choice for μ is given by

$$\mu(\varepsilon) = \begin{cases} 1, & \text{if} \quad \varepsilon < \Delta x, \\ 0, & \text{if} \quad \varepsilon \geq \Delta x, \end{cases}$$

or some smoothed version of it, (e.g., $\mu = \exp(-\varepsilon/\Delta x)$). For the diffusion term $\partial_{xx} p(u)$ we used the standard 2-nd order finite difference technique for second order time discretizations, and the standard 4-th order finite difference technique where 3-rd order time discretizations are used.

4 Numerical examples

In this section we test several second and third order IMEX R-K schemes that satisfy the above conditions and that are capable to capture the correct diffusion limit. We consider SPP2(3,3,2) scheme [31] as a second order IMEX R-K scheme of type A, ARS(2,2,2) scheme [1] as a second order IMEX R-K of type ARS. As third order IMEX R-K schemes here we consider ARS(4,4,3) scheme [1]. Note that ARS(2,2,2) and ARS(4,4,3) schemes satisfy the conditions required in the Definition 3 and in particular the additional conditions (18) are satisfied. Moreover we introduce here a new third order IMEX R-K scheme as example of type CK. This scheme has $s = 5$ internal stages, and it is stiffly accurate in the sense of Definition 3., i.e. $\tilde{b}^T = e_s^T \tilde{A}$ and $b^T = e_s^T A$. It is trivial to proof that the additional order conditions (18) are automatically satisfied for this type of scheme. We reproduced the coefficients of this scheme in Appendix 4. We called this scheme ARK3.

In all the computations presented in this paper we denote each scheme with IMEX *type-space discretization*. We remark that we use WENO scheme of 2-3 order and WENO scheme of 3-5 order [34] for the space discretization, then we will refer to as IMEX *type*-WENO23 or IMEX *type*-WENO35 respectively.

Note that for the converge test in order to test the second order IMEX RK schemes we used central differences schemes when $\varepsilon \to 0$ and all schemes tested have the prescribed order of accuracy in the limit case. We will refer to as *IMEX-type*-CdS. Of course, linear central differencing will fail to capture discontinuities in the initial conditions or nonlinearities in the flux. Such problems can be treated by adopting suitable WENO schemes.

For the sake of comparison we will also present results for IMEX *type*-WENO23 schemes, such as ARS(2,2,2) and SSP2(3,3,2) (namely second-order schemes) for the first test (see Table 1). Similar results have been obtained for the second numerical test.

4.1 Convergence test

First we test the convergence of these schemes considering a simple prototype system of hyperbolic systems (4). In the following tests we put $\varepsilon = 10^{-6}$ and we choose $\Delta t \approx \Delta x$.

For the first test we set $p(u) = u$ and $q(u) = 0$. Then we get

$$\begin{aligned} u_t &= -v_x - \mu u_{xx} + \mu u_{xx}, \\ \varepsilon^2 v_t &= -u_x - v, \end{aligned} \tag{20}$$

that in the limit case, $\varepsilon = 0$ and $\mu = 1$ leads to the linear diffusive problem

$$\begin{aligned} u_t &= u_{xx}, \\ u(x,0) &= u_0(x). \end{aligned}$$

We use periodic boundary conditions with $u_0(x) = \cos(x)$, and $x \in [0\ ,2\pi]$, so that $u(x,t) = u_0(x)\exp(t)$ is an exact solution. The results are reported in Table 1 showing that the expected convergence rates are reached for the u-component.

Next we set $p(u) = q(u) = u$ and consider the following system

$$\begin{aligned} u_t + v_x &= \mu u_{xx} - \mu u_{xx} \\ \varepsilon^2 v_t + \mu u_x &= -(v-u), \end{aligned}$$

where the limiting behavior is given by an advection-diffusion equation. We use periodic boundary conditions with the initial data $u(x,0) = \exp(-(1+\cos(x-\pi))/\sigma)$, $v(x,0) = u(x,0)(1 -$

Schemes	$e_s^T \tilde{A} = \tilde{b}^T$	N	$L_\infty(u)$	Order
ARS(2,2,2)-CdS	yes	20	7.800e-03	
		40	1.873e-04	2.05
		80	4.597e-04	2.02
		160	1.138e-04	2.01
		320	2.833e-05	2.00
SSP2(3,3,2)-CdS	no	20	2.906e-02	
		40	7.979e-03	1.86
		80	2.039e-03	1.96
		160	5.120e-04	1.99
		320	1.274e-04	2.00
ARS(2,2,2)-WENO32	yes	20	4.820e-03	
		40	1.492e-03	1.69
		80	4.124e-04	1.85
		160	1.082e-04	1.93
		320	2.760e-05	1.97
SSP2(2,2,2)-WENO32	no	20	4.697e-03	
		40	1.483e-03	1.66
		80	4.102e-04	1.85
		160	1.074e-04	1.93
		320	2.748e-05	1.96
ARS(4,4,3)-WENO35	yes	20	1.810e-02	
		40	3.365e-03	2.42
		80	5.349e-04	2.65
		160	5.960e-05	3.16
		320	5.968e-06	3.31
ARK3-WENO35	yes	20	1.639e-02	
		40	3.099e-03	2.40
		80	5.167e-04	2.58
		160	5.821e-05	3.14
		320	5.949e-06	3.29

Table 1: Convergence rate for u in L_∞-norm in the pure diffusive limit.

$\mu \sin(x-\pi)/\sigma)$ with $\sigma = 0.05$ and $\mu = 1$, on the spatial interval $[0, 2\pi]$, at the final time $t = 0.3$. As reference solution we use the truncated Fourier representation of the exact solution

$$U_{exa}(x,t) = \sum_{k=-\infty}^{+\infty} U_k(t) e^{ikx}, \quad V_{exa}(x,t) = \sum_{k=-\infty}^{+\infty} V_k(t) e^{ikx}$$

with $U_k(t)$ and $V_k(t)$ satisfying

$$\begin{aligned} \dot{U}_k &= -ikV_k, \\ \varepsilon^2 \dot{V}_k &= -ikU_k + U_k - V_k. \end{aligned}$$

The results are given in Table 2 showing that again the expected convergence rates are reached for the u-component by all schemes.

The above convergence analysis has been performed in the limit $\varepsilon \to 0$, therefore we might expect a degradation of the accuracy for intermediate regimes as in the case of hyperbolic

Schemes	$e_s^T \tilde{A} = \tilde{b}^T$	N	$L_\infty(u)$	Order
ARS(2,2,2)-CdS	yes	40	3.867e-03	
		80	9.457e-04	2.03
		160	2.330e04	2.02
		320	5.798e-05	2.00
SSP2(3,3,2)-CdS	no	40	2.615e-03	
		80	6.243e-04	2.06
		160	1.543e-04	2.01
		320	3.850e-05	2.00
ARS(4,4,3)-WENO35	yes	40	4.297e-04	
		80	5.770e-05	2.89
		160	7.922e-06	2.86
		320	1.256e-06	2.65
ARK3-WENO35	yes	40	8.300e-04	
		80	1.167e-04	2.83
		160	1.603e-05	2.86
		320	2.230e-06	2.85

Table 2: Convergence rate for u in L_∞-norm in the convection-diffusion limit.

relaxation when the classical order is greater then two [3, 6, 9]. Furthermore, from the practical point of view, the understanding of this phenomenon is essential in situations where one is interested in the construction of higher order methods.

We investigated numerically the convergence rate for a wide range of the parameter ε. To this aim we apply to the first test problem (20) second and third order IMEX R-K schemes introduced before. Numerical convergence rate is calculated by the formula

$$p = \log_2(E_{\Delta t_1}/E_{\Delta t_2}),$$

where $E_{\Delta t_1}$ and $E_{\Delta t_2}$ are the global errors computed with step $\Delta t_1 = \mathcal{O}(\Delta x)$, $\Delta t_2 = \Delta t_1/2$ and $N = 80,\ 160$.

Figures 1, 2 and 3 shows the convergence rates as a function of ε^2 using different values of ε ranging from 10^{-6} to 1. Second order schemes ARS(2,2,2)-CdS, SSP2(3,3,2)-CdS tested have the prescribed order of accuracy uniformly in ε^2, (see Fig. 1). Instead, WENO-based schemes such as ARS(2,2,2)-WENO23 and SSP2(3,3,2)-WENO23 present a degradation of accuracy at intermediate regimes (see Fig. 2 and 3). This phenomenon requires further investigation. Furthermore, a degradation of accuracy in intermediate regimes is observed for both the third order schemes ARS(4,4,3)-WENO35 and ARK3-WENO35. This results confirm the theoretical analysis developed for these IMEX R-K schemes in [3].

Recent results on the development of high-order IMEX R-K schemes for systems with hyperbolic relaxation which are able to handle uniformly the stiffness in the whole range of the relaxation time have been developed in [4, 6]. The development of these schemes is aided by the knowledge of extra order conditions in addition to the classical ones [9, 31], which ensure accuracy in time at the various order of the stiffness parameter ε [4]. A similar analysis could help improving the uniform accuracy in ε also in case of diffusive relaxation. This derivation will be in complete analogy to the derivation of the algebraic order conditions obtained in [4, 6]. Here we do not explore further this direction and we leave it for future researches.

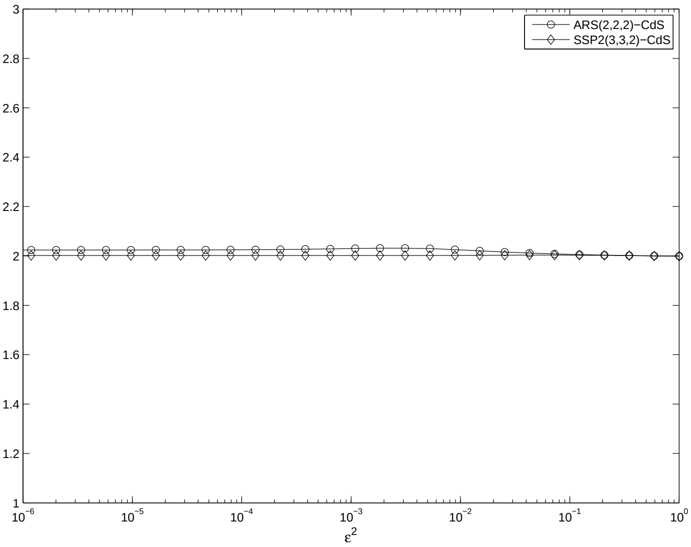

Figure 1: Convergence rate in L_∞-norm versus ε^2.

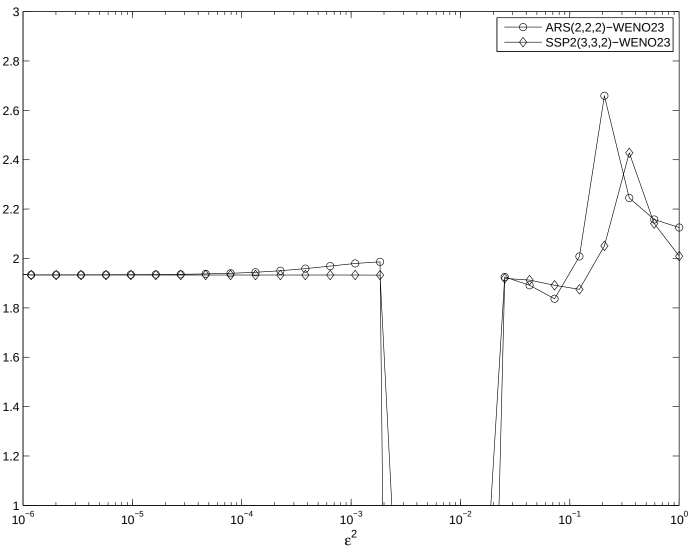

Figure 2: Convergence rate in L_∞-norm versus ε^2.

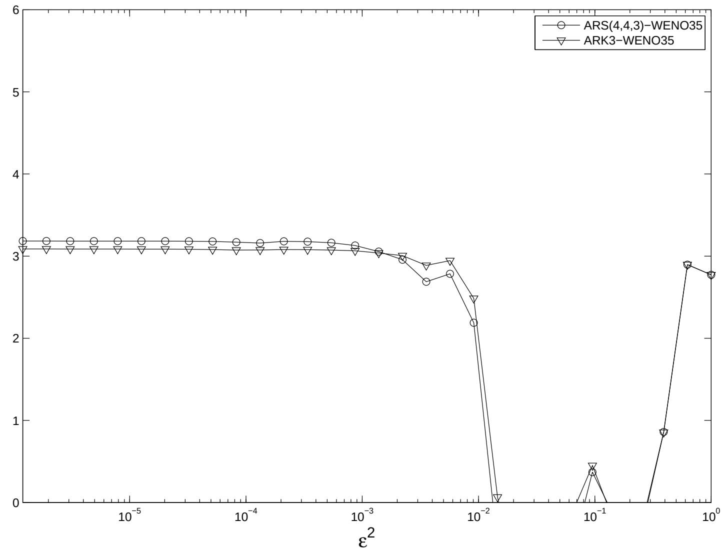

Figure 3: Convergence rate in L_∞-norm versus ε^2.

4.2 Shock test cases

In all the subsequent numerical tests we will consider the third order ARK3-WENO35 scheme. Now we apply the scheme to problems with discontinuous initial data, to show the shock capturing properties of the scheme.

First we consider a purely diffusive linear problem. We solve a Riemann problem, in the rarefied and diffusive regime for system

$$\begin{aligned} u_t + v_x &= \mu u_{xx} - \mu u_{xx} \\ \varepsilon^2 v_t + u_x &= -v. \end{aligned}$$

We take the following initial data

$$\begin{aligned} u_L &= 2.0 \quad v_L = 0, \quad -1 < x < 0, \\ u_R &= 1.0 \quad v_R = 0, \quad 0 < x < 1. \end{aligned}$$

As ε goes to zero we get $u_t = u_{xx}$, i.e. the problem becomes a classical Riemann problem for the heat equation.

In order to test our scheme we compute the numerical solution in the rarefied ($\varepsilon > \Delta x$) regime and in the diffusive ($\varepsilon \ll \Delta x$) regime. This means that when ε is very large (i.e., rarefied regime) μ is very small, and on the other hand when ε is very small (i.e., diffusive regime) μ is equal to 1.

We compute the scheme in the rarefied regime ($\varepsilon = 0.7$) and in the diffusive regime (or stiff regime) for $\varepsilon = 10^{-6}$. The numerical solution for u and v in the rarefied and diffusive regime are depicted with a reference solution obtained using a fine spatial grid of $N = 2000$ cells. The boundary condition are of reflecting type. The solution is reported at final time $t = 0.25$ in the rarefied regime and $t = 0.04$ in the diffusive regime. In Figures 4 and 5 we can observe that the scheme captures well the correct behavior of the the solutions both in rarefied regime where

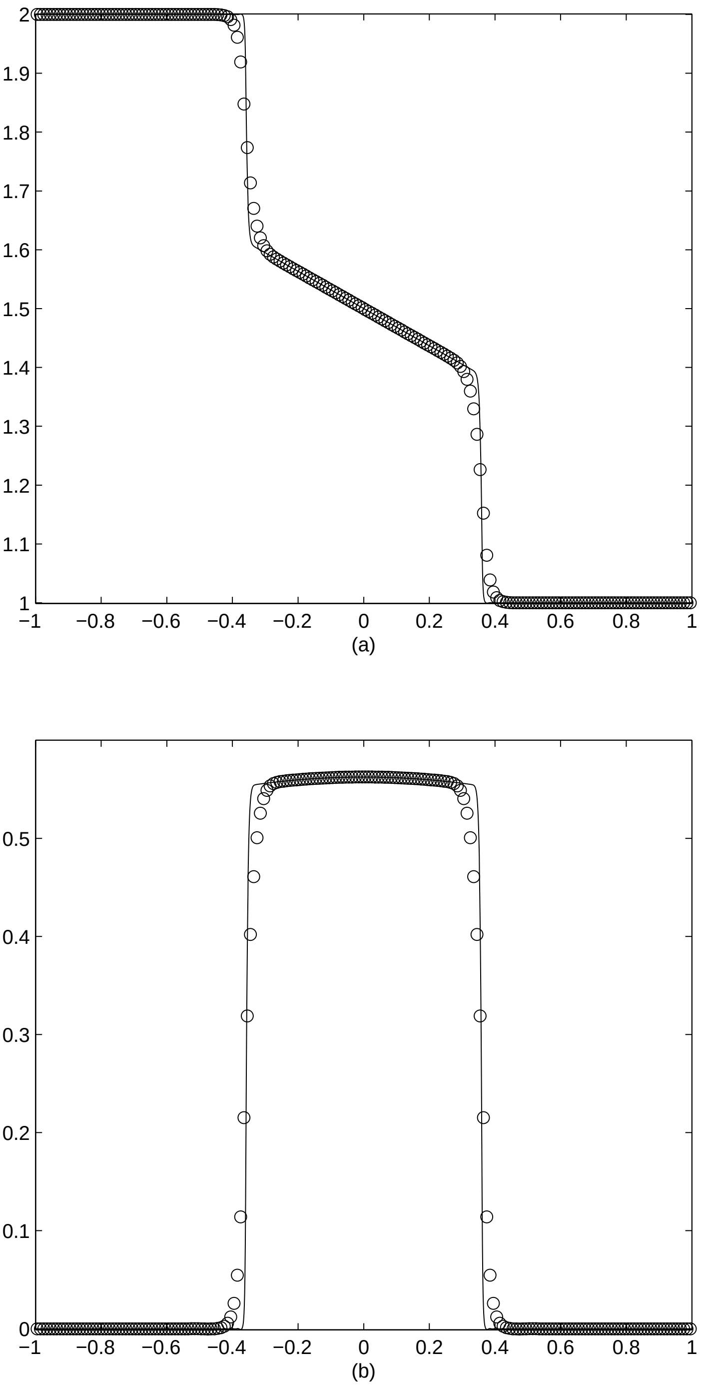

Figure 4: Numerical solution at time $t = 0.25$ in the rarefied regime ($\varepsilon = 0.7$) with $\Delta t = \lambda \Delta x$ with $\lambda = 0.5$ and $\Delta x = 0.01$. From the top to bottom the mass density u (a) and the flow v (b). Solid line is the 'exact' solution.

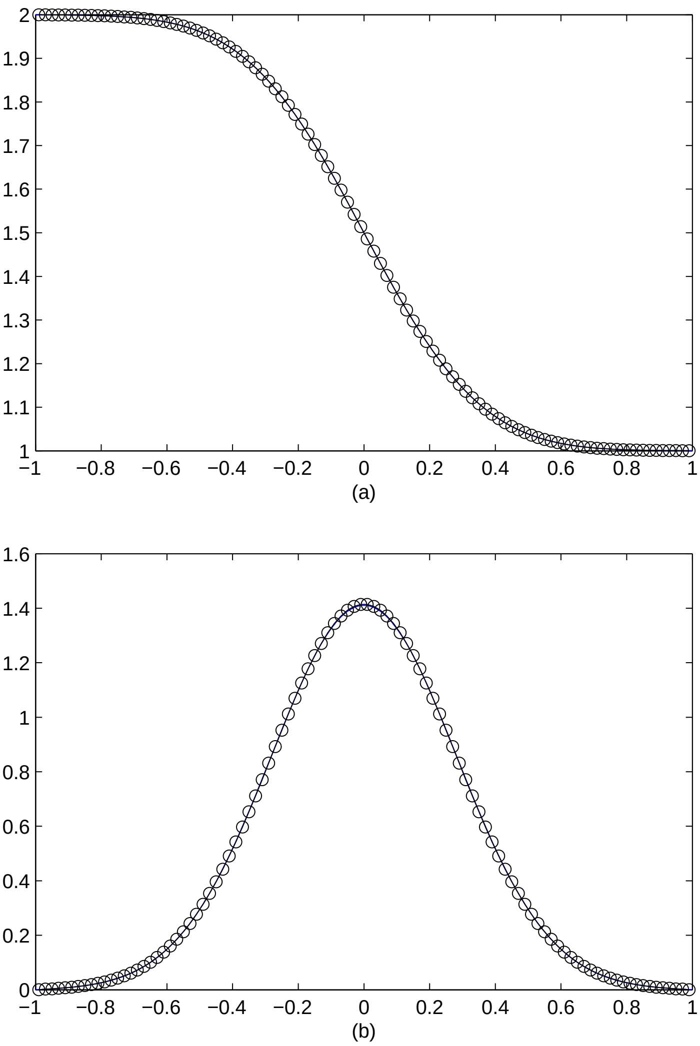

Figure 5: Numerical solution at time $t = 0.04$ in the parabolic regime ($\varepsilon = 10^{-6}$) with $\Delta t = \lambda \Delta x$ and $\lambda = 0.5$ and $\Delta x = 0.02$. From the top to bottom the mass density (a) u and the flow v (b). Solid line is the 'exact' solution.

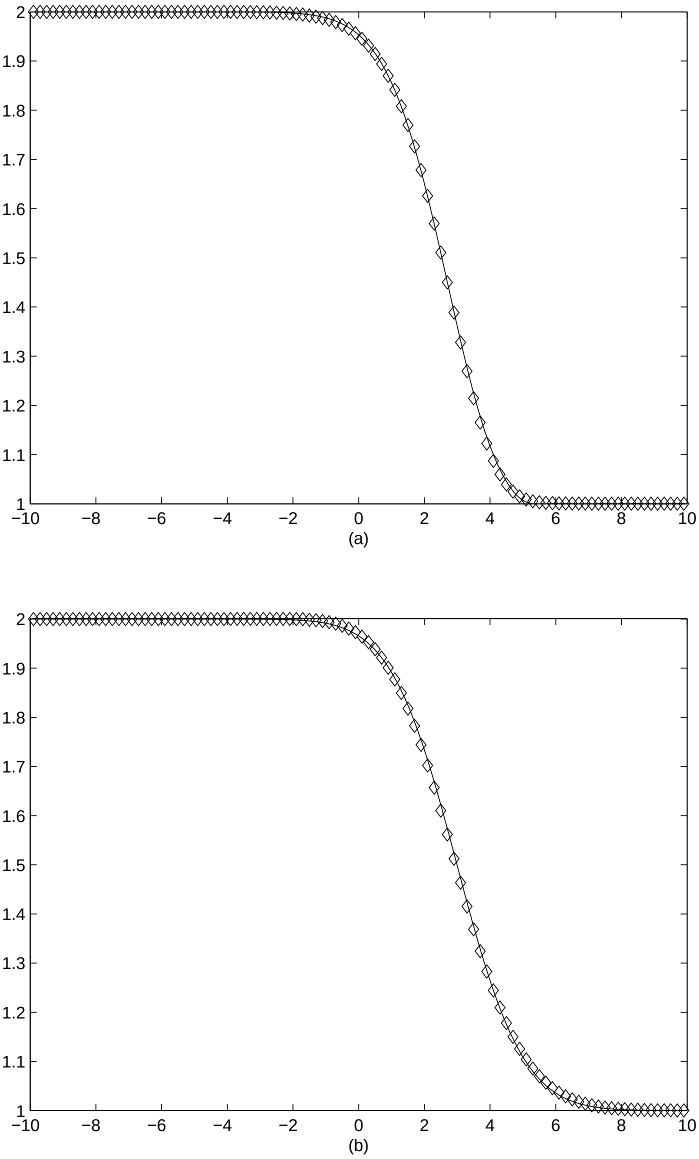

Figure 6: Numerical solution at time $t = 2.0$ in the (a) intermediate regime ($\varepsilon = 0.4$) and (b) parabolic regime ($\varepsilon = 10^{-6}$) with $\Delta t = \lambda \Delta x$ with $\lambda = 0.25$ and $\Delta x = 0.2$. Solid line is the exact solution.

it provides an accurate description of the shock without oscillations near the discontinuities and in the diffusive regime where the numerical solution matches accurately the reference solution.

Finally we consider the nonlinear Ruijgrok-Wu model, [32], (for details see [20])

$$\begin{aligned} u_t + v_x &= 0 \\ \varepsilon^2 v_t + u_x &= -2k_0 \left[v - \frac{C}{2}(u^2 - \varepsilon^2 v^2) \right] \end{aligned} \tag{21}$$

where C is a constant, i.e. $C = 1$. In the diffusive limit $\varepsilon \to 0$ the second equation provides

$$v = \frac{C}{2}u^2 - \frac{1}{2k_0}u_x,$$

and we get the limiting viscous Burgers equation

$$u_t + C\left(\frac{u^2}{2}\right)_x = Du_{xx}$$

with $D = 1/k_0$. The exact solution to the shock-wave problem has been given in [32]. The initial conditions are two local Maxwellians characterized by

$$\begin{aligned} u_L = 2.0, &\quad -10 < x < 0 \\ u_R = 1.0, &\quad 0 < x < 10, \end{aligned}$$

with $v = \left[(1 + u^2\varepsilon^2/2)^{1/2} - 1\right]/2\varepsilon^2$.

In Figure 6 we show the computed solution for the mass density u in the intermediate ($\varepsilon = 0.4$) and parabolic ($\varepsilon = 10^{-6}$) regimes versus the exact solution. As it can be seen once again, the scheme gives an accurate description of the viscous shock profiles.

5 Application to transport equations

In this section we apply the IMEX schemes derived in the first part of the manuscript to the case of neutron transport equations [23, 21, 27].

We consider the multidimensional dimension transport equation under the diffusive scaling. Let $f(t, \mathbf{x}, \mathbf{v})$ be the probability density distribution for particles at space point $\mathbf{x} \in \mathbb{R}^d$, time t, traveling with velocity $\mathbf{v} \in \Omega \subset \mathbb{R}^d$ with $\int_\Omega d\mathbf{v} = S$. Here Ω is symmetric in $\mathbf{v}$, meaning that $\int_\Omega g(\mathbf{v})d\mathbf{v} = 0$ for any function g odd in $\mathbf{v}$. Then f solves the linear transport equation

$$\varepsilon\partial_t f + \mathbf{v}\nabla_x f = \frac{1}{\varepsilon}\left(\frac{\sigma_s}{S}\int_\Omega f d\mathbf{v}' - \sigma f\right) + \varepsilon Q, \tag{22}$$

where $\sigma = \sigma(x)$ is the total cross section, $\sigma_s = \sigma_s(x)$ is the scattering coefficient. Here $Q = Q(x)$ is a source therm and ε the mean free path. Typically, $\sigma_s = \sigma - \varepsilon^2\sigma_A$ where $\sigma_A = \sigma_A(x)$ is the absorption coefficient. Such an equation arises in neutron transport [10], radiative transport [12] and wave propagation in random media [33], etc. In all these applications, the scaling appearing in (23) is typical, and gives rise to a diffusion equation as $\varepsilon \to 0$ of the form [21]

$$\partial_t \rho = \frac{1}{S}\int_\Omega \mathbf{v} \cdot \nabla_x \left(\frac{\mathbf{v}}{\sigma} \cdot \nabla_x \rho\right) d\mathbf{v} - \sigma_A \rho + Q,$$

where $\rho = \int_\Omega f\, d\mathbf{v}$.

5.1 Problem reformulation

Consider now the one-dimensional transport equation

$$\varepsilon \partial_t f + v \partial_x f = \frac{1}{\varepsilon} \left(\frac{\sigma_s}{2} \int_\Omega f d\mathbf{v}' - \sigma f \right) + \varepsilon Q, \tag{23}$$

$x_L < x < x_R$, and $-1 \leq v \leq 1$ with boundary conditions

$$\begin{aligned} f(t, x_L, v) &= F_L(v), \quad \text{for} \quad v > 0, \\ f(t, x_R, -v) &= F_R(v), \quad \text{for} \quad v > 0. \end{aligned} \tag{24}$$

In [21] the authors proposed a method based on the even-odd decomposition $f = r + \varepsilon j$ where $r = \frac{1}{2}(f(v) + f(-v))$ and $j = \frac{1}{2\varepsilon}(f(v) - f(-v))$, that splits the equation (23) as two equations, each for $v > 0$

$$\begin{aligned} \varepsilon \partial_t f(v) + v \partial_x f(v) &= \frac{1}{\varepsilon} \left(\frac{\sigma_s}{2} \int_{-1}^{1} f dv' - \sigma f(v) \right) + \varepsilon Q, \\ \varepsilon \partial_t f(-v) - v \partial_x f(-v) &= \frac{1}{\varepsilon} \left(\frac{\sigma_s}{2} \int_{-1}^{1} f dv' - \sigma f(-v) \right) + \varepsilon Q. \end{aligned} \tag{25}$$

Adding and subtracting these two equations leads to

$$\begin{aligned} \partial_t r + v \partial_x j &= -\frac{\sigma_s}{\varepsilon^2}(r - \rho) - \sigma_A r + Q, \\ \partial_t j + \frac{v}{\varepsilon^2} \partial_x r &= -\frac{\sigma_s}{\varepsilon^2} j - \sigma_A j, \end{aligned} \tag{26}$$

where

$$\rho = \int_0^1 r dv. \tag{27}$$

As $\varepsilon \to 0$, system (26) gives

$$r = \rho, \quad j = -(v/\sigma)\partial_x r.$$

Applying this in the first equation of (26) and integrating over v we get the diffusion equation

$$\partial_t \rho = \frac{1}{3} \partial_{xx} \rho - \sigma_A \rho + Q. \tag{28}$$

Remark. To get boundary conditions for r and j we use relations

$$r + \varepsilon j|_{x=x_L} = F_L(v), \quad r - \varepsilon j|_{x=x_R} = F_R(v). \tag{29}$$

When $\varepsilon \to 0$, $j = -(v/\sigma)\partial_x r$ then applying this in (29) one gets

$$r - \varepsilon v \partial_x r|_{x=x_L} = F_L(v), \quad r + \varepsilon v \partial_x r|_{x=x_R} = F_R(v). \tag{30}$$

Such boundary conditions will avoid a boundary layer in the limit case $\varepsilon \to 0$, therefore the numerical boundary conditions are obtained by dicretizing Eq. (30). As done in [21], the boundary conditions have been applied using a second order implementation of equation (29) based on central differences. Extensions to higher-order implementation of equations (30) and to different boundary conditions are not considered here and will be investigated in a forthcoming work. According to this, for our tests we chose a second order scheme in space and time, because the boundary conditions are discretized to second order accuracy.

Now we start from system (26) and, adding and subtracting the quantity $v^2\partial_{xx}r/\sigma$ in the first equation, we reformulate the problem in the equivalent form

$$\begin{aligned} \partial_t r &= \underbrace{-v\partial_x(j + \frac{\mu(\varepsilon)v\partial_x r}{\sigma})}_{Explicit} \underbrace{-\frac{\sigma_s}{\varepsilon^2}(r-\rho) - \sigma_A r + Q + \mu(\varepsilon)\frac{\partial_{xx}r}{\sigma}}_{Implicit}, \\ \partial_t j &= \underbrace{-\frac{1}{\varepsilon^2}(j + \frac{v\partial_x r}{\sigma})}_{Implicit}, \end{aligned} \tag{31}$$

The new system is then discretized in time using an IMEX R-K scheme as described in the first part of the manuscript. The implicit-explicit integration process is emphasized in (31).

We remark that this new formulation of the diffusive relaxation system (26) is such that when ε tends to zero the system relaxes towards (28). From a numerical point of view the new formulation has several advantages. In particular, as $\varepsilon \to 0$, the IMEX R-K scheme applied to system (31) originates a fully implicit scheme for solving the diffusion equation (28).

The equations are discretized in space and velocity, i.e. $r(x_i, v_m, t_n) \approx r^n_{i,m}$ where $\{v_m\}$ are chosen to be the N_v positive nodes of the Gauss-Legendre quadrature formula, with $2N_v$ nodes in the interval $[-1, 1]$ while $x_i = \Delta x(i - 1/2)$ for $i = 1, ..., N_p$. Note that the computation of the k-th stage of the implicit equation $r^{(k)}_{i,m}$, requires the quantity $\rho^{(k)}_i$ in the implicit part in (31). Such quantities are obtained as follows. Assume we have computed $r^{(l)}_{i,m}$ for $l = 1, ..., k-1$, then $r^{(k)}_{i,m}$ is obtained from

$$r^{(k)}_{i,m} = \overline{r}^{(k-1)}_{i,m} + \Delta t a_{kk}\left(\frac{\sigma_S}{\varepsilon^2}(r^{(k)}_{i,m} - \rho^{(k)}_i) - \sigma_A r^{(k)}_{i,m} + Q\right) \tag{32}$$

discretizing system (31) without the quantity $\mu(\varepsilon)v^2\partial_{xx}r/\sigma$ in the implicit and explicit part. The quantity $\overline{r}^{(k-1)}_{i,m}$ represents the explicit part (that we assume has already been computed). Then, in order to compute $\rho^{(k)}_i$ we apply Gauss quadrature on both sides of (32) (i.e. multiply by the weights w_m and sum over m), setting $\mu = 0$. In this way we obtain an equation for $\rho^{(k)}_i$ that can be explicitly solved, and such value is plugged in (31) in order to compute $r^{(k)}_{i,m}$.

5.2 Numerical results

In this section we shall consider some transport problems in slab geometry. We will present the transient and the steady state solutions. We remark that in all the test problems we have used $N_v = 8$ thus the standard 16 points Gaussian quadrature set for the velocity space. To obtain uniformly accurate second order schemes both space and time we combined the SSP2(3,3,2) second order IMEX R-K scheme with standard second order shock capturing WENO 3-2 scheme (see [34] for details), i.e. SSP2(3,3,2)-WENO23. We remark that we can obtain analogous results considering ARS(2,2,2)-WENO23. In all the test considered the initial distribution is $f(\mathbf{x}, \mathbf{v}, t = 0) = 0$.

We emphasize that, besides uniform accuracy in ε, our approach allows to choose larger time steps, since there is no stability restriction on the time step. As we will show, this permits to obtain numerical results presented in the actual literature at a lower computational cost. Nevertheless, in order to get an accurate resolution of the behavior of the solution, smaller time step may be necessary.

Depending on the regime of the parameter ε, we compare our numerical solution to a direct discretization of the diffusion limit (28) when ε tends to zero, whereas for intermediate values of the parameter ε we compute a reference solution using a much finer grid in space. We compare our new approach denoted as BPR versus the approach proposed by Jin et al., [21], called here JPT. We refer to [23, 27] for similar results. In all figures we use notations N_s and N_p to denote the number of time steps and grid points respectively.

Problem I:

$$\begin{array}{cccc} x \in [0,1], & & F_L(v) = 1, & F_R(v) = 0, \\ \sigma_S = 1, & \sigma_A = 0, & Q = 0, & \varepsilon = 10^{-8}. \end{array}$$

The numerical results are reported in figure 4 and 5 at different times $t = 0.01,\ 0.05,\ 0.15$, and at $t = 2$ where the steady state is reached. In this problem we see that in both cases, the results in the transient and steady state solutions show a good behaviour with the correct diffusion limit. We see that the schemes JPT and BPR are very close to the reference solution at any times.

Problem II: This is a two-material problem used in [21, 27, 23] where in the purely absorbing region $[0, 1]$ the solution decays exponentially whereas in the purely scattering region $[1, 11]$ the solution is diffusive, the parameters are the following

$$\begin{array}{c} x \in [0,11], \quad F_L(v) = 5, \quad F_R(v) = 0, \\ \sigma_S = 0, \quad \sigma_A = 1, \quad Q = 0, \quad \varepsilon = 1, \quad \text{for} \quad x \in [0,1], \\ \sigma_S = 1, \quad \sigma_A = 0, \quad Q = 0, \quad \varepsilon = 0.01, \quad \text{for} \quad x \in [1,11]. \end{array}$$

An interface layer is produced between the pure absorbing region and the scattering region. Two meshes are used in the domain $[0, 11]$, a thin mesh $\Delta x = 0.05$ in $[0, 1]$ and a coarse mesh $\Delta x = 1$ in $[1, 11]$, which means that between the interface layer we have to use a space discretization with a non uniform mesh. Finite difference can be used with non uniform mesh. We consider WENO approach for the reconstruction step and we proposed an extension to non uniform mesh for this test problem. We computed the coefficients, smoothness indicators and weights for a second order WENO(2,3) reconstruction.

At time $t = 150$ the solution has reached the steady state. We computed the reference solution with a very fine discretization using a uniform mesh in all the domain $[0, 11]$. The numerical schemes gives a good description for the solution in the absorption and diffusive regions, in fact, we observe that for the steady state, Figure 5 (bottom), scheme JPT and our scheme are close o the reference solution, except at the interface where a slight difference can be observed.

Problem III: Concerning this problem we present two different situations (see [27]), first in an intermediate regime with non-isotropic boundary conditions that generate a boundary layer:

$$\begin{array}{c} x \in [0,1], \quad F_L(v) = v, \quad F_R(v) = 0, \\ \sigma_S = 1, \quad \sigma_A = 0, \quad Q = 0, \quad \varepsilon = 10^{-2}. \end{array}$$

Second, in a more diffusive regime, since $\varepsilon = 10^{-4}$. However with a coarse discretization the boundary layer is not resolved, but we observe that the schemes are close to the reference solution inside the domain and accurately capture the solution inside the domain. The reference solution has been obtained using a fine discretization and the boundary layer is resolved. The results are plotted at time $t = 0.4$ in figure 6.

6 Conclusions

In this manuscript we have presented a general way to tackle diffusion limit for hyperbolic and kinetic problems which permits to obtain uniformly accurate schemes. The new approach, in particular, give rise to a fully implicit method for the diffusion component of the limiting system. This is obtained without solving nonlinear systems of implicit equations but by a suitable blending into the IMEX R-K method of a fully implicit solver for limiting diffusive system. Numerical results show that the schemes are able to capture the correct asymptotic behavior of the system at a lower computational cost compared to other approaches presented in the literature.

The method here presented is based on the use of IMEX Runge-Kutta methods however extension to more general additive Runge-Kutta schemes are naturally possible. In fact from our problem reformulation

$$\begin{aligned} u' &= \underbrace{f_1(u,v)}_{explicit} + \underbrace{f_2(u)}_{implicit}, \\ \varepsilon^2 v' &= \underbrace{g(u,v)}_{implicit} \end{aligned} \tag{33}$$

we can clearly combine different implicit solvers to tackle the "highly" stiff component $g(u, v)$ which originates the algebraic condition $g(u, v) = 0$ giving rise to the equilibrium projection $v = G(u)$ and the "mildly" stiff component $f_2(u)$ corresponding to the limiting diffusive term. We leave this possibility to future research directions.

7 Appendix

7.1 Stability analysis of first order IMEX schemes

For the subsequent analysis we restrict to the linear case $p(u) = u$ and $q(u) = 0$

$$\begin{aligned} u_t &= -(v + \mu u_x)_x + \mu u_{xx}, \\ \varepsilon^2 v_t &= -u_x - v, \end{aligned} \tag{34}$$

We now look for a Fourier solution of the form $u = \hat{u}(t)\exp(i\xi x)$, $v = \hat{v}(t)\exp(i\xi x)$ and inserting the *ansatz* into systems (1), the evolution equations are

$$\begin{aligned} \hat{u}_t &= -i\xi\hat{v} + \xi^2\mu\hat{u} - \xi^2\mu\hat{u} \\ \varepsilon^2\hat{v}_t &= -i\xi\hat{u} - \hat{v} \end{aligned} \tag{35}$$

It is convenient to rewrite the system using the variable $\hat{w} = -i\hat{v}/\xi$ in place of $\hat{v}$ so the system becomes

$$\begin{aligned} \hat{u}_t &= \xi^2(\hat{w} + \mu\hat{u}) - \xi^2\mu\hat{u}, \\ \varepsilon^2\hat{w}_t &= -\hat{u} - \hat{w}. \end{aligned} \tag{36}$$

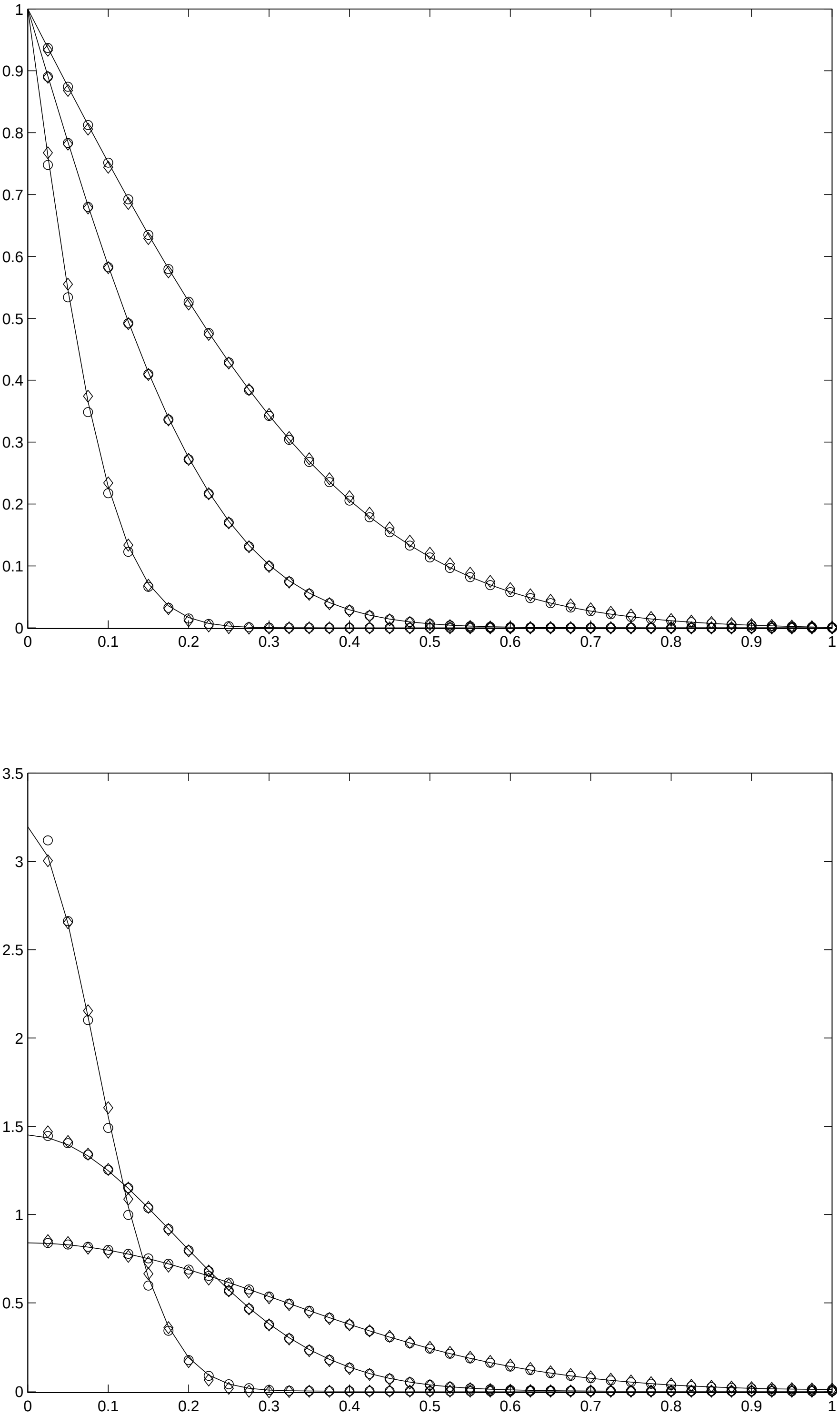

Figure 7: Top the mass density ρ, bottom the flux ρu. JPT ($\circ$), $\varepsilon = 10^{-6}$, $\Delta x = 0.025$, $\Delta t = 0.0002$, $N_s = 50, \quad 250, \quad 750$. BPR ($\Diamond$) $\Delta t = \lambda \Delta x$, $\lambda = 0.035$ $N_s = 11, \quad 57, \quad 171$. The exact diffusion solution is represented by the solid line.

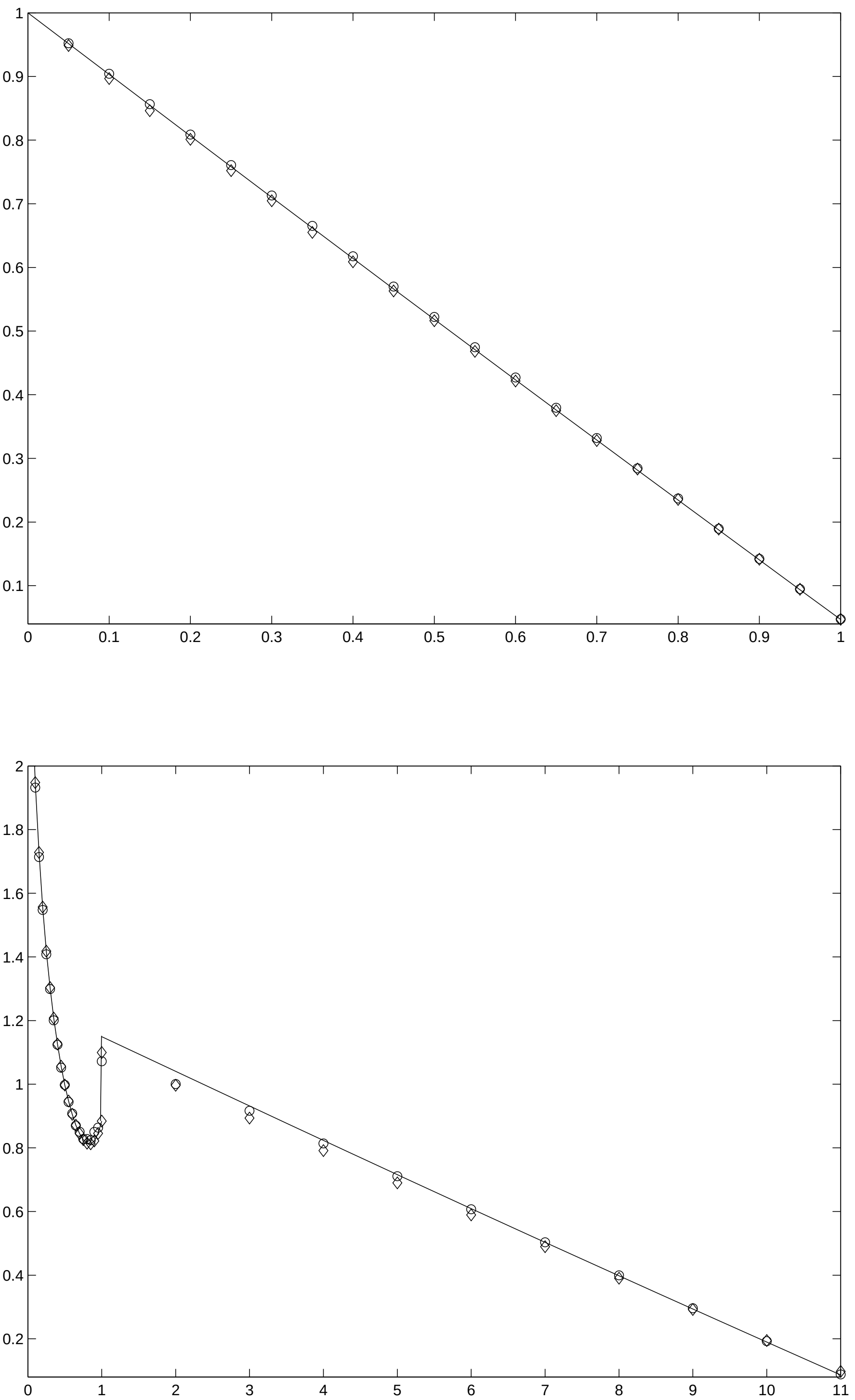

Figure 8: Top the mass density ρ, JPT ($\circ$), $\varepsilon = 10^{-6}$, $N_p = 20$, $\Delta t = 0.001$, $N_s = 2000$. BPR ($\lozenge$) $\Delta t = 0.0035$, $N_s = 561$. The *exact* solution is represented by the solid line. Bottom the steady state solution of the mass density ρ. JPT ($\circ$), $\varepsilon = 1$, $\Delta x = 0.05$ on $[0, 1]$, $\varepsilon = 0.01$, $\Delta x = 1$ on $[1, 11]$ and $\Delta t = 0.025$ with $N_s = 6000$. BPR ($\lozenge$) $\Delta t = \Delta x$, with $N_s = 3000$.

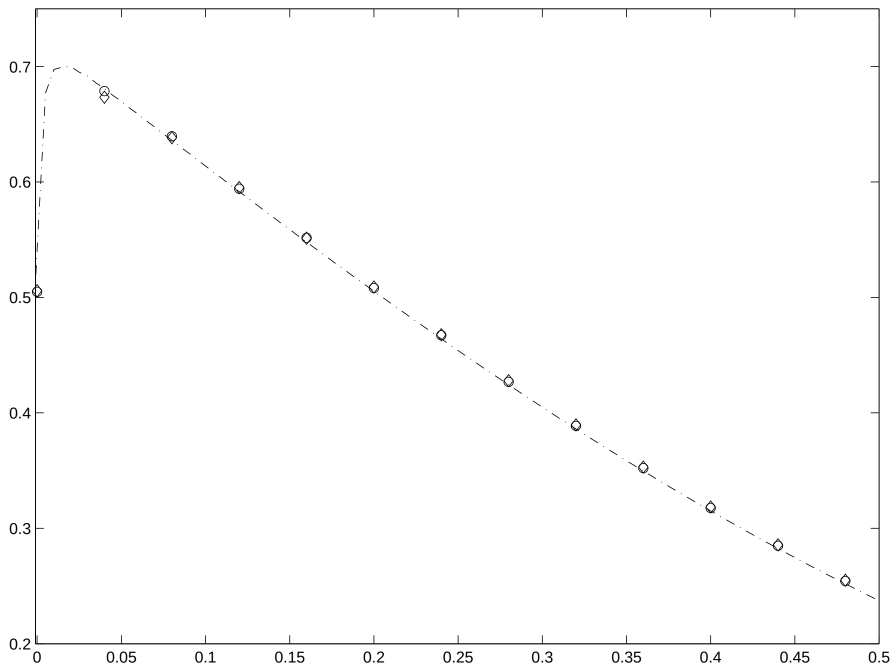

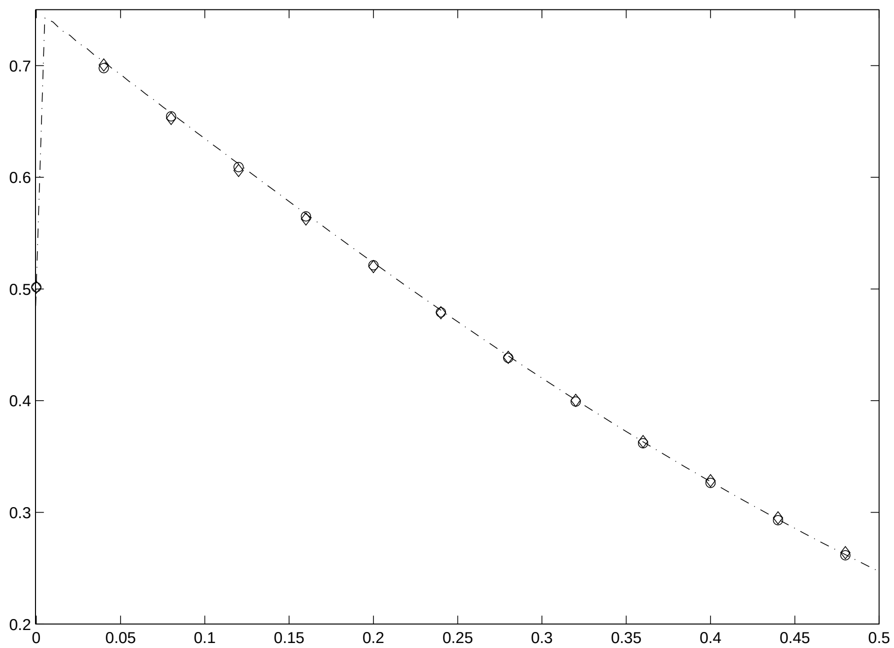

Figure 9: Steady state solution of the mass density ρ. Top, JPT ($\circ$), $\varepsilon = 10^{-2}$, $\Delta x = 0.04$, $\Delta t = 0.001$, $N_p = 25$, $N_s = 400$. BPR ($\Diamond$) $\Delta x = 0.04$, $\Delta t = 0.002$, $N_p = 25$, $N_s = 100$. Bottom $\varepsilon = 10^{-4}$. The reference solutions are represented by the dash dot line computed with BPR using $N_p = 400$.

We apply the first order IMEX method based on explicit and implicit Euler schemes to get

$$\begin{array}{rcl} \hat{u}^{n+1} & = & \hat{u}^n + \Delta t \xi^2 (\hat{w}^n + \mu \hat{u}^n) - \Delta t \xi^2 \mu \hat{u}^{n+1}, \\ \varepsilon^2 \hat{w}^{n+1} & = & \hat{w}^n - \Delta t \hat{u}^{n+1} - \Delta t \hat{w}^{n+1}, \end{array} \tag{37}$$

which after manipulation can be written explicitly in the form

$$\begin{array}{rcl} \hat{u}^{n+1} & = & \hat{u}^n + \dfrac{\Delta t \xi^2}{1 + \Delta t \xi^2 \mu} \hat{w}^n, \\ \hat{w}^{n+1} & = & \dfrac{\varepsilon^2 (1 + \Delta t \xi^2 \mu) - \Delta t^2 \xi^2}{(\varepsilon^2 + \Delta t)(1 + \Delta t \xi^2 \mu)} \hat{w}^n - \dfrac{\Delta t}{\varepsilon^2 + \Delta t} \hat{u}^n. \end{array} \tag{38}$$

In order to study the stability of the method we compute the eigenvalues of the stability matrix

$$R = \begin{pmatrix} 1 & \dfrac{\Delta t \xi^2}{1 + \Delta t \xi^2 \mu} \\ -\dfrac{\Delta t}{\varepsilon^2 + \Delta t} & \dfrac{\varepsilon^2 (1 + \Delta t \xi^2 \mu) - \Delta t^2 \xi^2}{(\varepsilon^2 + \Delta t)(1 + \Delta t \xi^2 \mu)} \end{pmatrix}. \tag{39}$$

We obtain the expressions

$$\lambda_\pm = \frac{1}{2} \left\{ 1 + \alpha(1+\beta) - \beta \pm \sqrt{[1 + \alpha(1+\beta) - \beta]^2 - 4\alpha} \right\} \tag{40}$$

with

$$\alpha = \frac{\varepsilon^2}{\varepsilon^2 + \Delta t}, \quad \beta = \frac{\Delta t \xi^2}{1 + \mu \Delta t \xi^2}.$$

It can be shown that $|\lambda_\pm| < 1$ when

$$\alpha < \frac{1 - 2\beta + \beta^2}{1 + 2\beta + \beta^2}.$$

The above inequality involves a third order polynomial in Δt

$$-\xi^4 (\mu - 1)^2 \Delta t^3 + 2\xi^2 (2\,\varepsilon^2 \xi^2 \mu + 1 - \mu) \Delta t^2 + \left(4\,\varepsilon^2 \xi^2 - 1\right) \Delta t < 0. \tag{41}$$

The roots of this polynomial are given by $T_0 = 0$ and

$$T_\pm = \frac{1}{(\mu - 1)^2 \xi^2} \left\{ 2\varepsilon^2 \xi^2 \mu - \mu + 1 \pm 2\varepsilon\xi \sqrt{\varepsilon^2 \xi^2 \mu^2 - \mu + 1} \right\}.$$

Condition (41) can be satisfied only if the last two roots are positive. This is guaranteed when $2\varepsilon\xi < 1$ and so we have the time step restriction $\Delta t < T_-$. The largest stability region is obtained when $\mu = 1$ for which we get

$$\Delta t < \frac{1}{4} \frac{(1 - 4\xi^2 \varepsilon^2)}{\varepsilon^2 \xi^4}, \tag{42}$$

where the right hand side is a decreasing function of ε^2.

7.2 Analysis of second order stiffly accurate schemes

Proposition 2 *Consider an IMEX Runge-Kutta scheme of type A. Then we proof that there exist no second-order tree stage scheme satisfying the conditions* $b^T A^{-1} = e_s^T$ *and* $\tilde{b}^T = e_s^T \tilde{A}$.

Proof. We consider the classical second order conditions

$$
\begin{aligned}
\tilde{b}^T e &= 1, \quad b^T e = 1, && (43)\\
\tilde{b}^T \tilde{c} &= 1/2, \quad b^T c = 1/2, && (44)\\
\tilde{b}^T c &= 1/2, \quad b^T \tilde{c} = 1/2, && (45)
\end{aligned}
$$

with $c = A\mathbf{1}$ and $\tilde{c} = \tilde{A}\mathbf{1}$ and the conditions $b^T A^{-1} = e_s^T$ and $\tilde{b}^T = e_s^T \tilde{A}$.
For $s = 3$ the Butcher *tableau* of a stiffly accurate IMEX R-K of type A is

$$
\begin{array}{c|ccc}
0 & 0 & 0 & 0\\
\tilde{c}_2 & \tilde{c}_2 & 0 & 0\\
1 & \tilde{b}_1 & \tilde{b}_2 & 0\\
\hline
 & \tilde{b}_1 & \tilde{b}_2 & 0
\end{array}
\qquad
\begin{array}{c|ccc}
\gamma & \gamma & 0 & 0\\
c_2 & c_2-\gamma & \gamma & 0\\
1 & b_1 & b_2 & \gamma\\
\hline
 & b_1 & b_2 & \gamma
\end{array}
$$

(note that stiff accuracy implies $c_s = \tilde{c}_s = 1$) and the resulting system of equations can be explicitly written

$$
\begin{array}{cc}
\tilde{b}_1 = 1 - \tilde{b}_2, & b_1 = 1 - \gamma - b_2,\\
\tilde{b}_2 \tilde{c}_2 = 1/2, & (1-\gamma-b_2)\gamma + b_2 c_2 = 1/2 - \gamma,\\
(1-\tilde{b}_2)\gamma + \tilde{b}_2 c_2 = 1/2, & b_2 \tilde{c}_2 = 1/2 - \gamma.
\end{array}
$$

In order to solve this system we can compute the coefficients as follows

$$
\tilde{b}_2 = 1/(2\tilde{c}_2), \quad b_2 = (1-2\gamma)/(2\tilde{c}_2),
$$

and

$$
\begin{aligned}
b_2(c_2-\gamma) &= 1/2 - 2\gamma + \gamma^2,\\
\tilde{b}_2(c_2-\gamma) &= 1/2 - \gamma.
\end{aligned}
$$

Substituting $\tilde{b}_2$ and b_2 we get

$$
\begin{aligned}
\frac{(c_2-\gamma)}{2\tilde{c}_2} &= \frac{1/2 - 2\gamma + \gamma^2}{1-2\gamma},\\
\frac{(c_2-\gamma)}{2\tilde{c}_2} &= 1/2 - \gamma.
\end{aligned}
$$

now, comparing and equating the two expressions we have $\gamma^2 = 0$, this yields that γ is zero and it is impossible because the matrix A is invertible.

7.3 Derivation of algebraic conditions for index 1 DAEs

Here we derive index 1 order conditions up to the second order for IMEX Runge-Kutta of type A. We refer the reader to [4] for a general theory of how to obtain these algebraic index 1 order conditions.

We consider the problem (8)

$$u' = \hat{f}_1(u) + \hat{f}_2(u), \quad \text{with} \quad u(t_0) = u_0 \tag{46}$$

and applying a one step of a IMEX Runge-Kutta of type A we get for the numerical solution

$$u_1 = u_0 + \Delta t \sum_{i=1}^{s} \left(\tilde{b}_i \hat{f}_1(U_i) + b_i \hat{f}_2(U_i) \right) \tag{47}$$

with internal stages

$$U_i = u_0 + \Delta t \left(\sum_{j=1}^{i-1} \tilde{a}_{ij} \hat{f}_1(U_j) + \sum_{j=1}^{i} a_{ij} \hat{f}_2(U_j) \right). \tag{48}$$

As usual we have denoted by $e = (1, \ldots, 1)^T$. Now in order to check the order of a IMEX Runge-Kutta, one has to compute the Taylor series expansion of the exact solution $u(t_0 + \Delta t)$ and the numerical one u_1 around to $\Delta t = 0$. This leads to algebraic conditions for the coefficients of the scheme. Then, expanding the exact and numerical solution into Taylor series and comparing them we can derive these conditions. Here we derive only order conditions up to the second order, an extension to the third order is trivial.
First of all we compute the higher derivatives of the exact solution u of (46) at the initial point t_0. For this, we have from (46), $u^{(q)} = (\hat{f}_1(u))^{(q-1)} + (\hat{f}_2(u))^{(q-1)}$ and this gives

$$\begin{aligned} &u'(t_0) = \hat{f}_1(u_0) + \hat{f}_2(u_0), \\ &u''(t_0)'' = \hat{f}_1'(u_0)(\hat{f}_1(u_0) + \hat{f}_2(u_0)) + \hat{f}_2'(u_0)(\hat{f}_1(u_0) + \hat{f}_2(u_0)) \end{aligned} \tag{49}$$

and so on. Now, turning to the numerical solution by putting $\Delta t \hat{f}_k(U_i) = K_{k,i}$ for $k = 1, 2$ we rewrite (47)-(48) as

$$U_i = u_0 + \sum_{j=1}^{i-1} \tilde{a}_{ij} K_{1,j} + \sum_{j=1}^{i-1} a_{i,j} K_{2,j}, \tag{50}$$

$$u_1 = u0 + \sum_{i=1}^{s} \left(\tilde{b}_i K_{1,i} + b_i K_{2,i} \right) \tag{51}$$

where $K_{1,i}$, $K_{2,i}$, U_i and u_1 are functions of Δt. Now, we develop the derivatives of $K_{k,i} = \Delta t \hat{f}_k(U_i)$ by a Leibniz' rule and we get $K_{k,i}^{(q)} = \Delta t (\hat{f}_k(U_i))^{(q)} + q(\hat{f}_k(U_i))^{(q-1)}$ for $k = 1, 2$. Consequently, this giver for $\Delta t = 0$

$$K_{k,i}^{'} = 1 \hat{f}_k(u_0),$$
$$K_{k,i}^{''} = 2 \hat{f}'_k(u_0) U_i',$$

and so on. Here the derivatives of K_i^k and U_i are evaluated in $\Delta t = 0$. Now by (50) using

$$U_i^{(q)} = \sum_{j=1}^{i-1} \tilde{a}_{ij} K_{1,j}^{(q)}(0) + \sum_{j=1}^{i} a_{ij} K_{2,j}^{(q)}(0),$$

we get

$$
\begin{aligned}
U_i' &= \sum_{j=1}^{i-1} \tilde{a} \hat{f}_1(U_j) + \sum_{j=1}^{i} a_{ij} \hat{f}_2(U_j), \\
U_i'' &= 2\sum_{j=1}^{i-1} \tilde{a}_{ij} \hat{f}_1(U_j)(\hat{f}_1(U_j) + \hat{f}_1(U)) + 2\sum_{j=1}^{i} a_{ij} \hat{f}_2(U_j)(\hat{f}_1(U_j) + \hat{f}_1(U_j)).
\end{aligned} \tag{52}
$$

about the derivatives of the internal stages. Now concerning the derivatives of the numerical solution we get

$$
u_1^{(q)} = \sum_{i=1}^{s} \left(\tilde{b}_i K_{1,i}^{(q)}(0) + b^T K_{2,i}^{(q)}(0) \right),
$$

and by (52) we obtain

$$
\begin{aligned}
u_1' &= \sum_{i=1}^{s} \left(\tilde{b}_i \hat{f}_1(u_0) + b_i \hat{f}_2(u_0) \right), \\
u_1'' &= 2\sum_{i=1}^{s} \tilde{b}_i \hat{f}'(u_0)(\sum_{j=1}^{i-1} \tilde{a}_{ij} \hat{f}_1(U_j) + \sum_{j=1}^{i} a_{ij} \hat{f}_2(U_j)) \\
&+ 2\sum_{i=1}^{s} b_i \hat{f}_2'(u_0)(\sum_{j=1}^{i-1} \tilde{a}_{ij} \hat{f}_1(U_j) + \sum_{j=1}^{i} a_{ij} \hat{f}_2(U)).
\end{aligned} \tag{53}
$$

Now in order to derive the order conditions we compare (49) and (53), then for the differential u-component we obtain the classical second order conditions and the coupling order one for a IMEX R-K scheme ([31, 9]).
Now we compute the derivatives of the solution v at the initial point t_0. Thus we consider $v = G(u)$ and we compute the derivatives by $v^{(q)} = (G(u))^{(q)}$ and this gives

$$
\begin{aligned}
&v' = G'(u_0)(\hat{f}_1 + \hat{f}_2), \\
&v'' = G''(u_0)(\hat{f}_1 + \hat{f}_2) + G'(u_0)(\hat{f}_1' \hat{f}_1 + \hat{f}_2' \hat{f}_2),
\end{aligned} \tag{54}
$$

and so on. In the last expression we have omitted the obvious arguments. Now we consider the numerical solution

$$
v_1 = R(\infty) v_0 + \sum_{i=1}^{s} b_i \omega_{ij} V_j,
$$

and its derivatives are $v_1^{(q)}(0) = \sum_{i=1}^{s} b_i \omega_{ij} V_j^{(q)}(0)$. Then by $V_i = G(U_i)$ we get $V_i'(0) = G'(u_0) U_i'(0)$ and it follows $V_j'(0) = G'(u_0) \left(\sum_{j=1}^{i-1} \tilde{a}_{i,j} \hat{f}_1 + \sum_{j=1}^{i} a_{ij} \hat{f}_2 \right)$.This means

$$
v_1'(0) = \sum_{i=1}^{s} b_i \omega_{ij} G'(u_0) \left(\sum_{j=1}^{i-1} \tilde{a}_{i,j} \hat{f}_1 + \sum_{j=1}^{i} a_{ij} \hat{f}_2 \right)
$$

then comparing this expression with the first in (54) we obtain the algebraic order conditions up to the second order where $\tilde{c}_i = \sum_{j=1}^{i-1} \tilde{a}_{ij}$ and $c_i = \sum_{j=1}^{i} a_{ij}$ with

$$
\sum_{i=1}^{s} b_i \omega_{ij} \tilde{c}_j = 1, \quad \sum_{i=1}^{s} b_i \omega_{ij} c_j = 1.
$$

This gives only the condition $\sum_{i=1}^{s} b_i \omega_{ij} \tilde{c}_j = 1$, instead the second condition is automatically satisfied. An extension to the third order is trivial.

7.4 Second and third order IMEX schemes

1. Second order IMEX schemes:

   - ARS(2,2,2) scheme, [1]

$$
\begin{array}{c|ccc}
0 & 0 & 0 & 0 \\
\gamma & \gamma & 0 & 0 \\
1 & \delta & 1-\delta & 0 \\
\hline
 & \delta & 1-\delta & 0
\end{array}
\qquad
\begin{array}{c|ccc}
0 & 0 & 0 & 0 \\
\gamma & \gamma & 0 & 0 \\
1 & 0 & 1-\gamma & \gamma \\
\hline
 & 0 & 1-\gamma & \gamma
\end{array}
$$

   with $\gamma = (2-\sqrt{2})/2$ and $\delta = 1 - 1/(2\gamma)$.

   - SSP2-(3,3,2) scheme, [31]

$$
\begin{array}{c|ccc}
0 & 0 & 0 & 0 \\
1/2 & 1/2 & 0 & 0 \\
1 & 1/2 & 1/2 & 0 \\
\hline
 & 1/3 & 1/3 & 1/3
\end{array}
\qquad
\begin{array}{c|ccc}
1/4 & 1/4 & 0 & 0 \\
1/4 & 0 & 1/4 & 0 \\
1 & 1/3 & 1/3 & 1/3 \\
\hline
 & 1/3 & 1/3 & 1/3
\end{array}
$$

2. Third order IMEX schemes:

   - ARS(4,4,3) scheme, [1]

$$
\begin{array}{c|ccccc}
0 & 0 & 0 & 0 & 0 & 0 \\
1/2 & 1/2 & 0 & 0 & 0 & 0 \\
2/3 & 11/18 & 1/18 & 0 & 0 & 0 \\
1/2 & 5/6 & -5/6 & 1/2 & 0 & 0 \\
1 & 1/4 & 7/4 & 3/4 & -7/4 & 0 \\
\hline
 & 1/4 & 7/4 & 3/4 & -7/4 & 0
\end{array}
\qquad
\begin{array}{c|ccccc}
0 & 0 & 0 & 0 & 0 & 0 \\
1/2 & 0 & 1/2 & 0 & 0 & \\
2/3 & 0 & 1/6 & 1/2 & 0 & 0 \\
1/2 & 0 & -1/2 & 1/2 & 1/2 & 0 \\
1 & 0 & 3/2 & -3/2 & 1/2 & 1/2 \\
\hline
 & 0 & 3/2 & -3/2 & 1/2 & 1/2
\end{array}
$$

   - ARK3 scheme

$$
\begin{array}{c|ccccc}
0 & 0 & 0 & 0 & 0 & 0 \\
1 & 1 & 0 & 0 & 0 & 0 \\
2/3 & 4/9 & 2/9 & 0 & 0 & 0 \\
1 & 1/4 & 0 & 3/4 & 0 & 0 \\
1 & 1/4 & 0 & 3/4 & 0 & 0 \\
\hline
 & 1/4 & 0 & 3/4 & 0 & 0
\end{array}
\qquad
\begin{array}{c|ccccc}
0 & 0 & 0 & 0 & 0 & 0 \\
1 & 1/2 & 1/2 & 0 & 0 & \\
2/3 & 5/18 & -1/9 & 1/2 & 0 & 0 \\
1 & 1/2 & 0 & 0 & 1/2 & 0 \\
1 & 1/4 & 0 & 3/4 & -1/2 & 1/2 \\
\hline
 & 1/4 & 0 & 3/4 & -1/2 & 1/2
\end{array}
$$

References

[1] U. Ascher, S. Ruuth, R. J. Spitheri, *Implicit-explicit Runge-Kutta methods for time dependent Partial Differential Equations*. Appl. Numer. Math. 25, (1997), pp. 151–167.

[2] M. Bennoune, M. Lemou, L. Mieussens, *Uniformly stable numerical schemes for the Boltzmann equation preserving the compressible Navier-Stokes asymptotic*, J. Comp. Phys., 227 (2008), 3781–3803.

[3] S. Boscarino, *Error Analysis of IMEX Runge-Kutta Methods Derided from Differential Algebraic Systems*, SIAM J. Numer. Anal. Vol. 45, No 4, pp. 1600-1621 (2007).

[4] S. Boscarino, *On an accurate third order implicit-explicit Runge-Kutta method for stiff problems*, Appl. Num. Math. 59 (2009) 15151528

[5] S. Boscarino, L. Pareschi, G. Russo, *IMEX Runge-Kutta schemes and hyperbolic systems of conservation laws with stiff diffusive relaxation*, ICNAAM, AIP Conference Proceedings 1168, (2009) 1106–1111.

[6] S. Boscarino, G. Russo, *On a class of uniformly accurate IMEX Runge-Kutta schemes and applications to hyperbolic systems with relaxation*, SIAM J. Sci. Comput., 31, 3, pp. 1926-1945, (2009).

[7] C. Buet, S. Cordier, *An asymptotic preserving scheme for hydrodynamics radiative transfer models*, Numerische Math. 108, 2, pp.199–221, (2007).

[8] J.A. Carrillo, T. Goudon, P. Lafitte, F. Vecil. *Numerical schemes of diffusion asymptotics and moment closures for kinetic equations*. J. Sci. Comput., 36, pp.113-149, (2008).

[9] M.H. Carpenter, C.A. Kennedy, *Additive Runge-Kutta schemes for convection-diffusion-reaction equations* Appl. Numer. Math. 44 (2003), no. 1-2, 139–181.

[10] K.M. Case, P.F. Zweifel, Linear Transport Theory. Addison-Wesley, Reading, MA (1997)

[11] F. Cavalli, G. Naldi, G. Puppo, M. Semplice, *High order relaxation schemes for non linear diffusion problems*. SIAM Journal on Numerical Analysis, pp. 2098-2119, 2007, Vol. 45, N. 5, ISSN: 0036-1429

[12] S. Chandrasekhar, Radiative transport. Dover, New York (1960)

[13] G. Q. Chen, D. Levermore, T. P. Liu, *Hyperbolic conservations laws with stiff relaxation therms and entropy*. Comm. Pure Appl. Math., 47, (1994), pp. 787–830.

[14] P. Degond, S. Jin, *A smooth transition model between kinetic and diffusion equations*. SIAM J. Numer. Anal., 42, 6, pp.2671-2687, (2005).

[15] L. Gosse, G. Toscani, *Asymptotic-preserving and well-balanced schemes for radiative transfer and the Rosseland approximation*. Numer. Math., 98, 2, pp.223-250, (2004).

[16] J. L. Graveleau, P. Jamet, *A finite difference approach to some degenerate nonlinear parabolic equations*. SIAM J. Appl. Math., 20 (1971), pp. 199–223.

[17] E. Hairer, G. Wanner, Solving Ordinary Differential Equation II: stiff and Differential Algebraic Problems. Springer Series in Comput. Mathematics, Vol. 14, Springer-Verlag 1991, Second revised edition 1996.

[18] E. Hairer, S. P. Norsett, G. Wanner, Solving Ordinary Differential Equation I: Nonstiff Problems. Springer Series in Comput. Mathematics, Vol. 8, Springer-Verlag 1987, Second revised edition 1993.

[19] S. Jin, F. Filbet, *A class of asymptotic preserving schemes for kinetic equations and related problems with stiff sources*, J. Comp. Phys. 229, 7625-7648, 2010.

[20] S. Jin, L. Pareschi, G. Toscani, *Diffusive Relaxation Schemes for Multiscale Discrete-Velocity Kinetic Equations* SIAM J on Numer. Anal., Vol. 35, No. 6 (Dec., 1998), pp. 2405-2439

[21] S. Jin, L. Pareschi, G. Toscani, *Uniformly accurate diffusive relaxation schemes for transport equations*. SIAM J. Numer. Anal., 38, 3, pp.913-936, (2000).

[22] S. Jin, L. Pareschi, *Discretization of the multiscale semiconductor Boltzmann equation by diffusive relaxation schemes*. J. Comp. Phys., 161, pp.312–330, (2000).

[23] A. Klar, *An asymptotic-induced scheme for non stationary transport equations in the diffusive limit*. SIAM J. Numer. Anal. 35, no. 3, (1998), pp. 1073–1094.

[24] A. Klar, *A numerical method for kinetic semiconductor equations in the drift-diffusion limit*. SIAM Journal on Scientific Computing, 20, 5, pp.1696-1712, (1998).

[25] A. Klar, *An asymptotic preserving numerical scheme for kinetic equations in the low mach number limit*. Siam J Numer Anal, 36, 5, pp.1507-1527, (1999).

[26] P. Lafitte, G. Samaey, *Asymptotic-preserving projective integration schemes for kinetic equations in the diffusion limit*, preprint (2010).

[27] M. Lemou, L. Mieussens, *A new asymptotic preserving scheme based on micro-macro formulation for linear kinetic equations in the diffusion limit*. SIAM Journal on Scientific Computing, 2010, vol. 31, no. 1, pp. 334-368.

[28] T. P. Liu, *Hyperbolic conservation laws with relaxation*, Comm. MAth. Phys. 108, (1987), pp. 153-175.

[29] G. Naldi, L. Pareschi, *Numerical Schemes for Hyperbolic Systems of Conservation Laws with Stiff Diffusive Relaxation* SIAM J. on Numer. Anal., Vol. 37, No. 4 (2000), pp. 1246-1270

[30] G. Naldi, L. Pareschi, *Numerical schemes for kinetic equations in diffusive regimes* App. Math. Letters, Vol. 11, (1998), pp. 29–35

[31] L. Pareschi, G. Russo, *Implicit-Explicit Runge-Kutta schemes and applications to hyperbolic systems with relaxations.* Journal of Scientific Computing Volume: 25, Issue: 1, October, 2005, pp. 129-155

[32] W. Ruijgrok, T.T. Wu, *A completely solvable model of the nonlinear Boltzmann equation.*, Phys. A, 113 (1982), pp. 401-416.

[33] L. Ryzhik, G. Papanicolaou, J.B. Keller *Transport equations for elastic and other waves in random media* Wave motion 24 (1996), pp. 327-370

[34] C-W. Shu, *Essentially Non Oscillatory and Weighted Essentially Non Oscillatory schemes for hyperbolic conservation laws*, in Advanced numerical approximation of nonlinear hyperbolic equations, Lecture Notes in Mathematics, 1697, (2000).

[35] A.N. Tikhonov, A.B. Vasl'eva, A.G. Sveshnikov, Differential Equations, Trans. from the Russian by A.B. Sossinskij, Springer Verlag, 1985, 238pp.